



Versatile crop yield estimator

Yuval Sadeh¹ · Xuan Zhu¹ · David Dunkerley¹ · Jeffrey P. Walker² · Yang Chen³ · Karine Chenu⁴

Accepted: 11 June 2024 / Published online: 22 July 2024
© The Author(s) 2024

Abstract

Accurate production estimates, months before the harvest, are crucial for all parts of the food supply chain, from farmers to governments. While methods have been developed to use satellite data to monitor crop development and production, they typically rely on official crop statistics or ground-based data, limiting their application to the regions where they were calibrated. To address this issue, a new method called VeRsatile Crop Yield Estimator (VeRCYe) has been developed to estimate wheat yield at the pixel and field levels using satellite data and process-based crop models. The method uses the Leaf Area Index (LAI) as the linking variable between remotely sensed data and APSIM crop model simulations. In this process, the sowing dates of each field were detected (RMSE = 2.6 days) using PlanetScope imagery, with PlanetScope and Sentinel-2 data fused into a daily 3 m LAI dataset, enabling VeRCYe to overcome the traditional trade-off between satellite data that has either high temporal or high spatial resolution. The method was evaluated using 27 wheat fields across the Australian wheatbelt, covering a wide range of pedo-climatic conditions and farm management practices across three growing seasons. VeRCYe accurately estimated field-scale yield ($R^2 = 0.88$, RMSE = 757 kg/ha) and produced 3 m pixel size yield maps ($R^2 = 0.32$, RMSE = 1213 kg/ha). The method can potentially forecast the final yield ($R^2 = 0.78$ – 0.88) about 2 months before the harvest. Finally, the harvest dates of each field were detected from space (RMSE = 2.7 days), indicating when and where the estimated yield would be available to be traded in the market. VeRCYe can estimate yield without ground calibration, be applied to other crop types, and used with any remotely sensed LAI information. This model provides insights into yield variability from pixel to regional scales, enriching our understanding of agricultural productivity.

Keywords Yield estimating · Crop model · Planting date · Harvest date · Yield map · Yield forecasting · Leaf Area Index · Wheat

1 Introduction

Scalable, reliable, and consistent crop yield forecasts are a key component to monitor and manage global food security (Nakalembe et al. 2021). Therefore, estimates of production as far ahead of harvest as possible can be of great value

to the futures markets as well as to farmers, governments, and food distribution agencies (Becker-Reshef et al. 2020; Hammer et al. 2001; Benami et al. 2021). Importantly, climate variability and extreme weather events are projected to increasingly affect future crop yields, potentially leading to an era of uncertainty in the global food system and severe food crises (Ray et al. 2015; Hammer et al. 2001; Feng et al. 2020). Spaceborne remote sensing is considered a reliable, affordable, large-scale, and timely source of data to improve crop yield estimation (Becker-Reshef et al. 2020). Therefore, numerous yield estimation methods using satellite data have been developed in the last few decades (e.g. Franch et al. 2015; Idso et al. 1977; Prasad et al. 2006; Ferencz et al. 2004).

Many approaches exist for estimating crop yields using remote sensing (Lobell 2013; Moulin et al. 1998) and can be divided into three groups: vegetation indices (VI), machine learning (ML), and data assimilation.

✉ Yuval Sadeh
yuval.sadeh@monash.edu

¹ School of Earth, Atmosphere and Environment, Monash University, Clayton, Victoria 3800, Australia

² Department of Civil Engineering, Monash University, Clayton, Victoria 3800, Australia

³ Department of Transport and Planning, Land Use Victoria, Melbourne, Victoria 3002, Australia

⁴ Queensland Alliance for Agriculture and Food Innovation, The University of Queensland, Toowoomba, Queensland 4350, Australia

1. VI-based methods are built on the correlation between VIs and crop yield (e.g. Raun et al. 2001; Labus et al. 2002; Bognár et al. 2017; Becker-Reshef et al. 2010). However, relying on an exclusive linear relationship identified in one region to provide yield estimates across other regions with variable environmental conditions may be problematic, particularly where the crops might be under stress resulting from low soil moisture, high ambient temperatures, or severe frost (Chenu et al. 2013; Ababaei and Chenu 2020; Zheng et al. 2015).
2. ML-based techniques for crop yield estimation have become very popular in the last decade (e.g. Kamir et al. 2020; Jeffries et al. 2019; Feng et al. 2020; Cai et al. 2019). However, these methods require a great amount of ground data obtained in different ways, including yield, sowing (planting) dates, soil properties, farm management practices, and weather for training and calibrating the model. Such data is rarely available for yield estimation over larger scales, such as at the regional or national level (Feng et al. 2020), and therefore, these ML-based models are calibrated locally. While locally calibrated yield estimation methods may achieve good accuracy of yield estimation, the use of these methods is limited to the area in which they were calibrated.
3. Data assimilation techniques are used to assimilate plant and soil observations into a prediction model to improve the simulation of crop development and estimate yield. These techniques are used to combine remotely sensed data with a dynamic model (such as a crop model) to reduce the uncertainties from both the model and the remotely sensed observations (Houser et al. 2012; Zhang et al. 2022; Prévot et al. 2003). However, these data assimilation techniques often require local calibration through field measurements (Manivasagam et al. 2021; Pan et al. 2019; Zhang et al. 2022; Beyene et al. 2022), which is one of the main drawbacks of this approach.

Despite the growing availability of Earth observation data to monitor crop development and yield estimation, the use of spaceborne sensors is limited by the type of data they can retrieve. For example, optical remote sensing cannot “see” through the crop canopy or the soil surface, but it can provide valid information about canopy chlorophyll content (Gitelson et al. 2005). Synthetic-aperture radar (SAR) can provide complementary data on the roughness, slope, geometry, and moisture of the soil surface (Sadeh et al. 2018; Walker et al. 2004). Conversely, crop growth models can be used to simulate the main physiological processes, which include the phenology stage, leaf and grain development, uptake of nutrient and water, biomass status, and response to abiotic stresses (Huang et al. 2019; Holzworth et al. 2014; Chenu et al. 2017). Therefore, merging the capabilities of remote sensing with crop model simulations has a

great potential for improving capabilities in monitoring crop development and yield estimation through time and space (Donohue et al. 2018; Chen et al. 2020).

One of the ways to blend the abilities of crop models and remotely sensed data is through the incorporation of the Leaf Area Index (LAI) observations into the crop growth model using data assimilation techniques (Ines et al. 2013; Pan et al. 2019; Huang et al. 2019, 2015; Zhang et al. 2022). LAI has been found to be a good indicator of phenological stage and leaf abundance, as well as crop status, and can be used as an indicator of different farm management practices, or biotic and abiotic stresses (Huang et al. 2019).

To remove the need for ground-based calibration, Lobell et al. (2015) devised a new and innovative method, named the SCYM (scalable satellite-based crop yield mapper). This method uses region-specific crop model simulations and gridded weather data to build a relationship between simulated crop yield and remotely sensed VIs using a multiple variable linear regression (Azzari et al. 2017; Lobell et al. 2015; Dado et al. 2020; Deines et al. 2021). In the process, Lobell et al. (2015) used the Agricultural Production Systems sIMulator (APSIM) (Holzworth et al. 2014) to produce a large number of model simulations that cover a representative range of climate, soil, and management settings for a specified region. Despite the potential of this innovative approach, it is not built to run in a forecast mode, and its operational capability in predicting crop yield is limited, particularly in smallholder farms (Nakalembe et al. 2021).

For decades, remotely sensed applications have been limited by the trade-off between high temporal and high spatial resolution satellite data, restricting their ability to estimate crop yield at the field and sub-field levels (Waldner et al. 2019). For example, the attempt to map yield on a large scale using light use efficiency models as proposed by Marshall et al. (2018) and Dong et al. (2020) showed promising results, but it is unable to estimate field and sub-field-scale yield. In order to fill that gap, a number of companies developed and launched Earth-observing CubeSats to a low Earth orbit, such as the Planet Labs’ PlanetScope (PS) constellation. However, constellations of CubeSats, exemplified by Planets PS, frequently exhibit somewhat different individual radiometric characteristics (Houborg and McCabe 2016, 2018; Sadeh et al. 2019; Leach et al. 2019). Recent studies (e.g., Jin et al. 2017a; Jain et al. 2016; Waldner et al. 2019; Manivasagam et al. 2021) show a strong improvement in the prediction accuracy when using higher spatiotemporal resolution datasets, but the potential of using such a unique high spatiotemporal resolution LAI dataset (Sadeh et al. 2021) to improve yield estimation and forecasting has yet to be fully evaluated.

While most studies estimated crop yield at regional, state, or national levels (e.g., Ines et al. 2013; Jin et al. 2017b, 2019; Azzari et al. 2017; Huang et al. 2015; Cai et al. 2019), only a few of these studies have tried to estimate

yield without ground calibration data (e.g., Lobell et al. 2015; Azzari et al. 2017; Jin et al. 2019; Becker-Reshef et al. 2010; Franch et al. 2015). Moreover, few studies have tried to estimate yield at the field and sub-field scales (e.g., Lai et al. 2018; Manivasagam et al. 2021; Donohue et al. 2018; Sagan et al. 2021; Chen et al. 2020) or have attempted to do so without any ground-based data for calibration (e.g., Burke and Lobell 2017; Jain et al. 2016; Deines et al. 2021; Dado et al. 2020), achieving limited success. To overcome these limitations, it has been proposed that new methods combining Earth observation data with crop growth model predictions are required in order to eliminate the need for *in situ* yield measurement and to provide a tool for global yield monitoring (Waldner et al. 2019).

One important management practice that greatly influences crop development, growth, and yield is the sowing date, as it affects the environmental conditions that the crops will experience during the growing season (Coventry et al. 1993; Flohr et al. 2017). While sowing represents the start of the growing season, the harvest typically occurs soon after crop maturity, at the end of the growing season. Sowing dates are a key input in crop models to explore how different management practices might affect yield (Flohr et al. 2017; Zheng et al. 2012; Chenu et al. 2017). Any uncertainty in the sowing date can affect model performance, and it is therefore important to have the best possible estimates of the sowing date (Mathison et al. 2017).

A new approach for sowing date detection using Planet's PlanetScope imagery reported 85% of successful sowing detection rate and an RMSE of 0.9–1.9 days (Sadeh et al. 2019). This method is based on identifying changes on the fields' surface; it can theoretically also be applied for detecting harvest dates. Data on harvest status is important for preparing for transportation of the grains (Shang et al. 2020) from the farm to the silos, and from there by train or truck to the port to be exported by ships, which can help to optimize import-export business opportunities (Amherdt et al. 2021).

In light of the above, this study sought to devise a new approach to the prediction of crop yields across a range of scales from pixels to entire fields that would require no ground-based data at all. The proposed method was tested on wheat, being an agricultural commodity that has an important place in global food production. Wheat is primarily cultivated in semi-arid regions of the world, rendering it highly vulnerable to climate variability (Hammer et al. 2001; Chenu et al. 2011), hence the importance of predicting its yield. This current study also (i) tested the ability of using field-level detected sowing dates as a crop model input and evaluate its contribution to the crop yield estimation accuracy; (ii) explored the possibility of using a high spatiotemporal resolution LAI time series to identify the best-representing model simulation out of thousands of possible simulations, to determine field-scale yield; (iii) generated yield maps at 3

m pixel size within the field; and (iv) tested the feasibility of modifying the sowing date detection method of Sadeh et al. (2019) to detect the timing of harvest.

2 Material and methods

This study developed a new method, designated VeRCYe—VeRsatile Crop Yield Estimator (pronounced “versi”), for estimating crop yield at the field and sub-field scales. VeRCYe uses LAI as the linking variable between remotely sensed (RS) data and APSIM's plant development and yield prediction (Fig. 1). It includes three main steps:

1. Identification of cultivated fields and the date on which they were sown using a CubeSat-based method (Sadeh et al. 2019).
2. Fusion of PlanetScope (PS) images and Sentinel-2 (S2) images to create daily LAI datasets having 3-m resolution (Sadeh et al. 2021).
3. Coupling of the sowing dates and LAI datasets with the APSIM-Wheat crop model to estimate wheat yield at the field scale.

The accuracy of the estimated yield was compared to the field-level yield from 27 fields (with an average size of 175 ha), as reported by farmers, including 21 fields obtained from the National Paddock Survey (Lawes et al. 2021). Fields were located in five Australian States, thereby incorporating diverse soils, weather conditions, farm management practices, and wheat cultivars. Field-level data from three growing seasons (2017–2019) were analyzed, including 22 fields with both a sowing date and a yield map generated by the combine harvester, and for 20 fields, a reported harvest date.

2.1 Sowing date detection

This part of the study aimed to generate reliable, field-level sowing dates for use as an input to the crop model simulation. In order to extract the sowing dates for each field, the semi-automated sowing date detection method proposed by Sadeh et al. (2019) was implemented. This method identifies sowing dates by using Planet's PlanetScope data to detect changes on the fields' surface caused by no-tillage sowing, through the implementation of principal component analysis (PCA). The PCA was conducted independently for each image, encompassing all four bands (RGB-NIR). This analysis yielded four principal components: PC₁, PC₂, PC₃, and PC₄. Sadeh et al. (2019) found that PC₁ was systematically the best PC to represent the variance in the soils and therefore the best to be used for sowing detection. In contrast

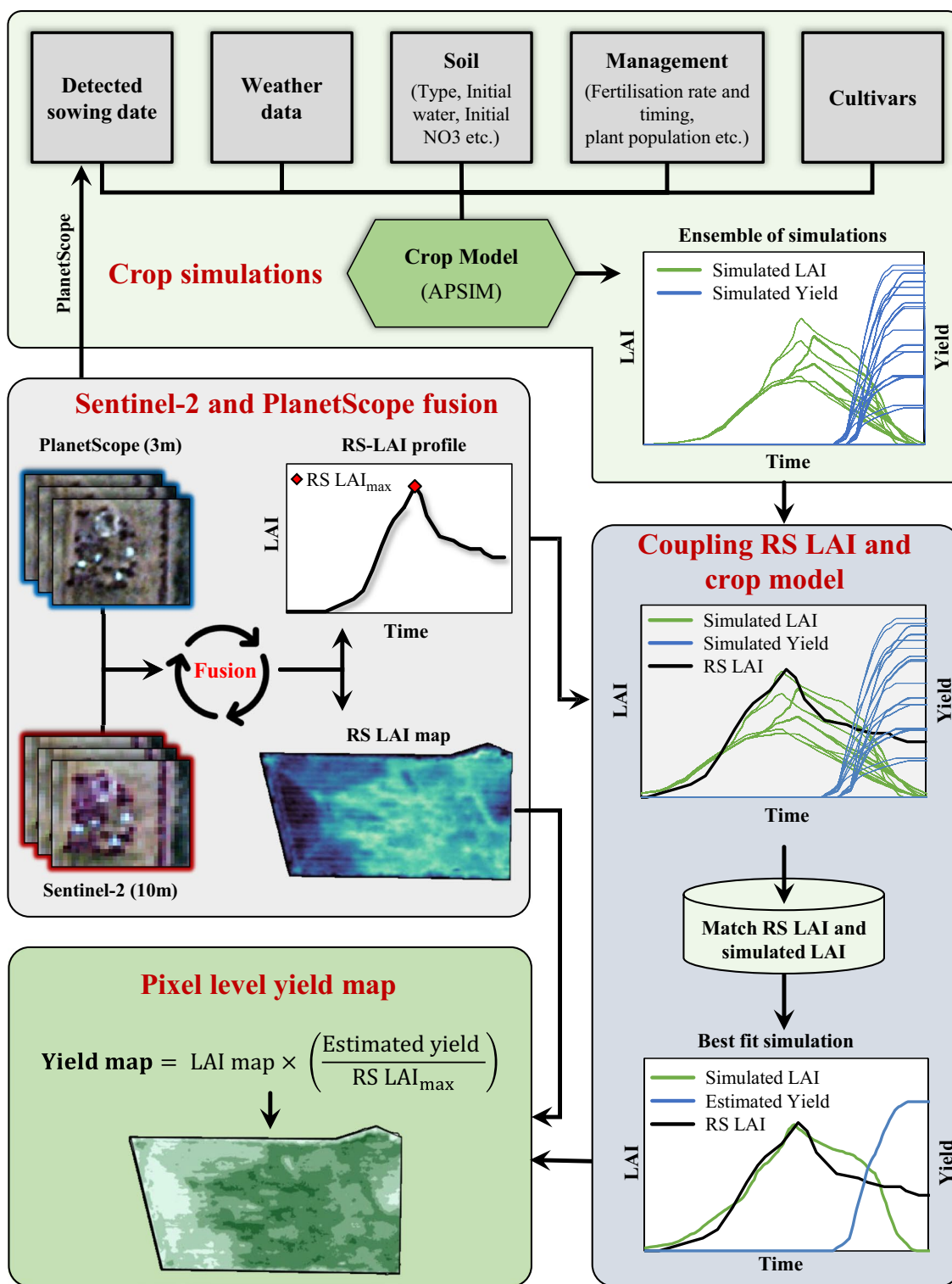


Fig. 1 VeRcSatellite Crop Yield Estimator (VeRCYe) yield estimation workflow, illustrating the integration of remotely sensed (RS) Leaf Area Index (LAI) with a crop simulation model.

to Sadeh et al. (2019), the current study used the following equation as it provided improved performance:

$$\text{Change} = \text{Image}_{t_2}^{\text{PC}_1} - \text{Image}_{t_1}^{\text{PC}_1}, \quad (1)$$

where $\text{Image}_{t_1}^{\text{PC}_1}$ is the first principal component of the earlier satellite image and $\text{Image}_{t_2}^{\text{PC}_1}$ is the first principal component of the later satellite image. The accuracy of the detection was evaluated against the dates reported by farmers.

To evaluate the contribution of using the detected sowing dates as model inputs, this study used the sowing window approach of Waldner et al. (2019). The sowing criterion that was used to initiate crop sowing was precipitation of ≥ 12 mm over 3 days or more, irrespective of soil moisture from 26 April to 15 July (this study used ≥ 12 mm instead of ≥ 15 mm as originally used by Waldner et al. (2019)). If the sowing criterion was not met during the sowing window, the crop was automatically sown on 15 July. The model's simulation start dates were determined by setting them to be 10 days prior to the detected sowing dates for each individual field.

2.2 APSIM model simulations

APSIM is an advanced simulation framework designed to model and simulate biophysical processes in agricultural systems. It is highly regarded for its ability to simulate a wide range of crops under a range of management practices and environmental conditions. APSIM models the biological and physical processes of agricultural systems at the field scale (Holzworth et al. 2018, 2014). It simulates crop growth and development (e.g., phenology, leaf area growth,

biomass accumulation, and yield) and soil processes (e.g., soil water balance, soil nitrogen, and carbon cycles) and simulates the impact of weather conditions and the effects of various management practices (e.g., irrigation, fertilizer application, and tillage) on agricultural production. APSIM utilizes a comprehensive set of input data to generate precise agricultural simulations, encompassing meteorological metrics (temperature, rainfall, solar radiation, humidity, wind speed), extensive soil profiles (texture, depth, water capacity, nutrients, pH, organic matter), specific crop details (variety, sowing density, growth stages), and management practices (sowing, irrigation, fertilization, and harvesting schedules) (Holzworth et al. 2018, 2014). However, APSIM does not incorporate modeling of diseases, pest infestations, or nutrient deficiencies, except those related to nitrogen.

The APSIM next-generation crop model (Holzworth et al. 2018) allows the running of numerous scenarios that represent a realistic range of farm management practices and environmental conditions (Table 1). This helps to overcome gaps in knowledge of farm management practices used in specific fields. In this process, ~ 2000 simulations of APSIM-Wheat were produced for each field (Fig. 1). The weather data were sourced from the closest weather station (www.bom.gov.au/), and the soil properties were from the four nearest soils available in the APSoil database (www.apsim.info/apsim-model/apsoil/). Each APSIM simulation outputs daily crop characteristics including LAI as well as a grain yield estimation

Table 1 Inputs used to run APSIM simulations at each studied field.

Inputs	Values/rules	Sources/references
Constant		
Sowing date	The detected sowing date	Sadeh et al. 2019
Sowing depth	30 mm	National Paddock Survey Lawes et al. 2021
Row spacing	25 cm	National Paddock Survey Lawes et al. 2021
Accumulated rainfall required for sowing	12 mm	
Duration of rainfall accumulation	7 days	
Changing/factorials		
Weather data (temperature, rainfall, solar radiation)	From the nearest weather station	Australian Bureau of Meteorology
Cultivars	Early, mid, and late-maturing local cultivars	Zheng et al. 2015 and National Paddock Survey
Plant population	50, 100, 150 plants per m ²	Chenu et al. 2013 and National Paddock Survey
Soil characteristics	The nearest 4 soils	APSoil database
Initial soil water	20%, 50%, 100% of the plant's available water capacity from the soil	
Fertilization at sowing	30, 50, 100 N kg/ha	Chenu et al. 2013
Fertilization at Zadok Stage—31 (stem elongation stage)	0, 30, 60 N kg/ha	Chenu et al. 2013
Fertilization at Zadok Stage—40 (booting stage)	0, 30 N kg/ha	Chenu et al. 2013

(kg/ha). Simulations that best reflected the LAI evolution were selected using an automatic rule-based algorithm (described below) to estimate the likely final yield. The range of plausible scenarios for each studied field is summarized in Table 1.

2.3 Remotely sensed LAI

As S2 was unlikely to provide cloud-free images every 5 days, this study used the newly developed method of Sadeh et al. (2021) to fuse PS and S2 imagery into daily 3 m LAI to generate a time series of LAI for each of the fields analyzed. In this process, images sourced from PS (with a spatial resolution of ~ 3 m, and a daily revisit time) and S2 (resolution of 10 m and 5-day revisit time) were fused to create daily, S2-consistent crop Green LAI at 3-m resolution; the Green LAI refers to the leaves which are photosynthetically active (Daughtry et al. 1992). The motivation to use the fused dataset was based on the assumption that high spatiotemporal resolution time series will improve the ability to monitor the crop development and therefore improve the yield estimates at the field and sub-field levels. In this process, (i) S2-based LAI data were generated using the Biophysical Processor module embedded within ESA's Sentinel Application Platform (SNAP) software (Louis et al. 2016; Weiss and Baret 2016), (ii) the PS and S2 RGB-NIR bands were fused into daily 3 m surface reflectance images, (iii) a VI was calculated based on the fused images, and (iv) the VI images were converted to LAI using a linear regression between the VI images and the S2-LAI time series. This fusion was conducted over the region of interest with the regression model self-adjusting through space and time (Sadeh et al. 2021).

This study tested the ability of using both the original remotely sensed LAI time series (the output of the fusion process), being equivalent to the generic S2-LAI product (but in 3 m daily datasets), and the improved remotely sensed LAI dataset, which adjusted the generic S2-LAI product estimations to better estimate wheat Green LAI (Sadeh et al. 2021). The adjustment of LAI values was achieved by "fine-tuning" from the generic S2-LAI images. This refinement utilized second-order polynomial regressions, which were found by Sadeh et al. (2021) to be the optimal method for representing the correlation between the in situ Green LAI and the values estimated remotely for a given vegetation index. In addition, for each of these datasets, this study investigated which of the 13 different VIs tested by Sadeh et al. (2021) to fuse PS and S2 into high spatiotemporal resolution LAI, resulted in the best performance for the VeRCYe approach. The VIs tested were as follows: NDVI, EVI2, MTVI2, MSAVI, WDRVI-Green, WDRVI, GCVI, OSAVI, GSR, GNDVI, RDVI, TVI, and SR. For more details, please refer to Sadeh et al. (2021).

2.4 Coupling APSIM simulations with remotely sensed LAI

Unlike many of the data assimilation-based methods which incorporate the RS LAI into the crop model (e.g. Manivasagam et al. 2021; Zhang et al. 2022), here, ~ 2000 different APSIM simulations were generated for each field, spanning a realistic range of possible on-farm and environmental variables (Table 1). Simulations most probable to accurately estimate the yield of the field of interest were selected based on a comparison between the patterns of the simulated LAI and the RS LAI during the growing season. The selection process includes five steps:

Step 1. Calculating for each APSIM simulation the following variables:

- (a) The gap in LAI between the maximum (max) simulated and RS LAI.
- (b) The gap in days between the timing of max simulated LAI and max RS LAI.
- (c) The RMSE between simulated and RS Green LAI, representing the stages when the leaves are photosynthetically active (Daughtry et al. 1992), in the range of 1 to max RS LAI (before the season's LAI peak).
- (d) The RMSE between simulated and RS Senescence-LAI, representing the stages when the leaves are not photosynthetically active (Delegido et al. 2015), in the range between the max RS LAI and 1 (after the season's LAI peak).

Step 2. Selecting only the simulations with the lowest 20% gap in LAI between the maximum (peak) simulated and RS LAI.

Step 3. Selecting from the simulations selected in step 2, only the simulations with a gap in days between the timing of the max simulated and RS LAI that is within a range of ± 5 days. If none of the simulations comply with this rule, then the selection range is increased to ± 10 days gap between the timing of the max simulated and RS LAI. If still none of the simulations meet this rule, then the range is increased by an additional ± 5 days until the criterion is met.

Step 4. Identifying the best fit simulated LAI to the RS LAI. However, this constantly resulted in underestimation of the estimated yield; the simulations which ended with high accuracy of yield estimation (in comparison to the reported yield) frequently had higher simulated LAI during the senescence period than the RS Senescence-LAI. This suggested that the RS Senescence-LAI failed to accurately estimate the true LAI of the crop, which aligned with the findings of Sadeh et al. (2021) that estimating wheat LAI at the senescence stage using the S2-LAI product achieved poor results in comparison with its Green

LAI estimations. An illustration of the underestimation of the RS Senescence-LAI compared to in situ LAI measurements (collected using the SunScan Canopy Analysis System) is shown in Fig. 2.

In order to overcome the underestimation of the RS Senescence-LAI, the simulations that continue for the next step must be simulations with the highest 20% of the average Senescence-LAI (of the selected simulations in the final step). The threshold of 20% resulted from sensitivity tests conducted to evaluate which percentage of the RMSE between the simulated Senescence-LAI and the RS Senescence-LAI typically performed best in this process. The sensitivity tests aimed to identify the smallest possible percentage in order to minimize the sample size of the data analyzed to save processing time. A breakdown of the simulated LAIs and their associated yield estimation is shown in Fig. 3. Here, the remaining 389 APSIM simulations (out of ~ 2000 initial simulations), which resulted from the gap in max LAI value and timing filters (steps 2 and 3 above) are plotted. In Fig. 3, the simulations whose estimated yield ended above the average of all 389 simulations are colored more darkly (dark green for simulated LAI and dark blue for its associated estimated yield) than the simulations whose estimated yield ended to be below the average (light green for simulated LAI and light blue for its associated estimated yield). Figure 3 shows no clear trend of which simulation resulted in a higher, and therefore more accurate, yield estimation at the Green LAI stage. However, at the senescence stage, a clear trend was found, with the simulations having a low Senescence-LAI more likely to result in lower yield estimation. The result of this rule (step 4) is presented in Fig. 4B.

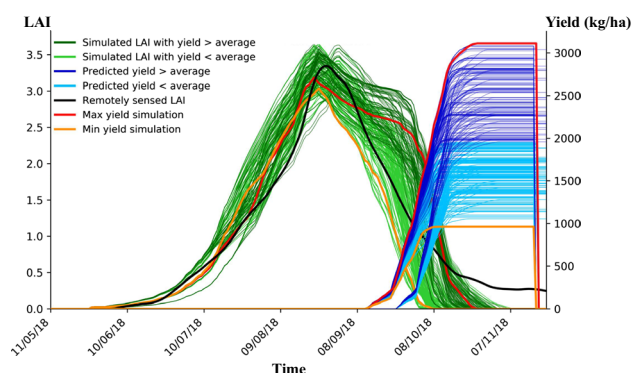


Fig. 3 A breakdown of the simulated Leaf Area Index (LAI) and their associated yield estimation after applying the gap in max LAI value and timing filters, which resulted in 389 selected simulations (out of ~ 2000). This figure shows a comparison of simulated and remotely sensed (RS) maximum LAI for the simulations fall within $\pm 10\%$ of the RS maximum LAI values and ± 5 days of the peak timing.

Step 5. Finally, estimating the field-scale yield as the mean of the simulations with the lowest 20% RMSE between simulated and RS Green LAI. An example of the output of the field-scale yield prediction is shown in Fig. 4C. In order to cover different scenarios, if step 4 results in fewer than 10 simulations, then the estimated yield is set as the mean of all these 10 simulations, i.e., without applying step 5.

In the scenario of an extremely low yield, such as during a severe drought, the ability to accurately estimate LAI using satellites is very limited. While crop models still simulate crops with very low LAI in such scenarios, the extremely underdeveloped crop surrounded by bare soil is typically associated with a reduced RS LAI owing to the mixed pixel effect

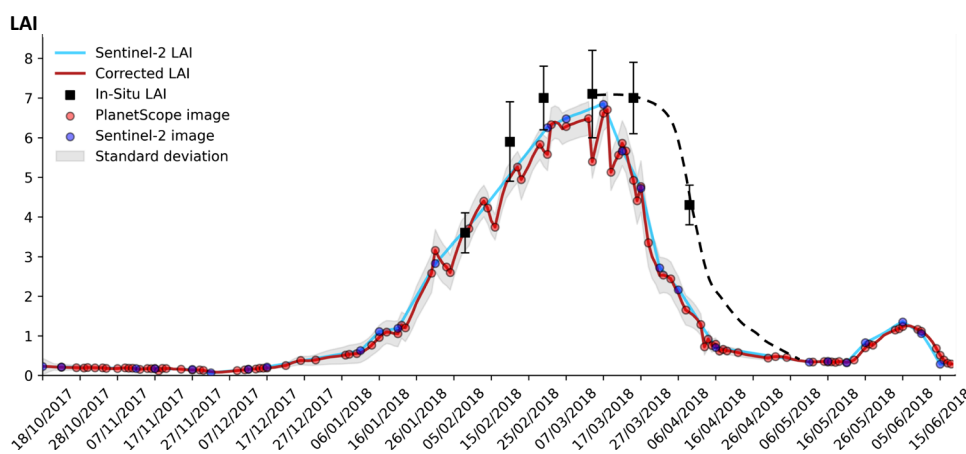
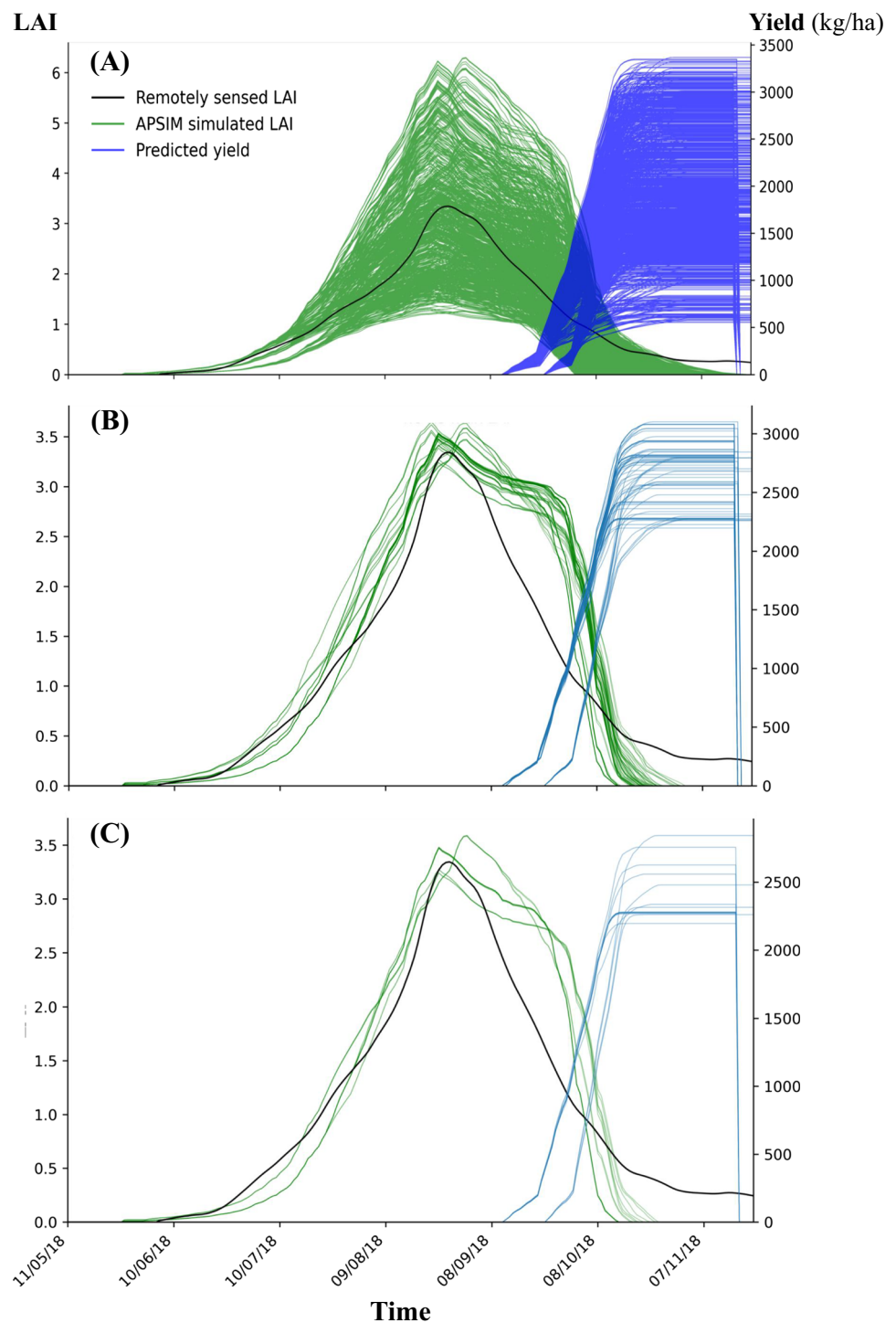


Fig. 2 An illustration of the underestimation of the remotely sensed (RS) Senescence Leaf Area Index (LAI) (blue and red lines) in comparison to the in situ Senescence-LAI (dashed black line). RMSE is presented (i) between the fused images LAI and in situ LAI measurements (“fused LAI–in situ RMSE”) and (ii) between the fused images

LAI and the Green LAI in situ measurements only (“fused LAI–in situ Green LAI RMSE”). The RMSE for the comparison between fused LAI and in situ LAI is 1.69, whereas the RMSE for fused LAI versus in situ Green LAI stands at 1.17.

Fig. 4 An example of how the best-fit simulations are identified out of thousands of different simulations of APSIM that were generated for a field, spanning a realistic range of possible on-farm and environmental variables. The green lines represent the simulated Leaf Area Index (LAI), and the blue lines represent the associated yield predictions, while the remotely sensed LAI in black. **A** The initial ~ 2000 APSIM simulations; **B** the outcome of steps 2–4, where only simulations within $\pm 10\%$ of the remotely sensed (RS) max LAI and ± 5 days are selected (78 simulations in this example); and **C** the output of field-scale yield estimation, when the estimated yield is determined based on all the simulations which met all the criteria (steps 1–5). Reported yield, 2618 kg/ha; estimated yield, 2394 kg/ha; error, -224 kg/ha; estimated yield standard deviation (STDV), 198 kg/ha; number of best-fit simulations, 16.



(Gao et al. 2012). Such crops typically have a very low yield and therefore should be addressed as a worst-case scenario. Consequently, in case that the maximum RS LAI of the season was lower than 0.9, the estimated yield is set as the mean of the three simulations with the lowest yield estimation.

The threshold selected to trigger the “severe drought” methodology was selected (i) based on the limited ability of spaceborne remotely sensed data to sense the undeveloped

crops in such a scenario; this is mainly owing to the sparse vegetation cover during a severe drought, and (ii) based on in situ evaluation of wheat fields during the 2018 drought in South-East Australia, using LAI-2000 Plant Canopy Analyzer (LI-COR), which was later compared with the RS LAI data to affirm the validity of the selected LAI threshold.

The proposed method was not developed using yield or LAI data of the 27 fields analyzed in this study; however,

one field was studied in depth to have a good understanding of the differences of the simulated LAI and RS LAI datasets. In addition, a similar process was used for two fields with extremely low yield, to understand the limitation of RS LAI to monitor crop development in severe drought conditions and APSIM's ability to simulate similar LAI values in such conditions. All the other fields analyzed were blindly tested as independent data. This study evaluated VeRCYe performance in two modes, yield estimation at the end of the season and in-season forecasting mode. The end of the season yield estimation mode uses the whole LAI time series of the growing season (i.e., 100% of the LAI data). The performance of this mode was evaluated more extensively both at field and pixel levels as this was the main scope of this study. The forecasting mode in this study operated in a way that it would provide a preliminary indication if VeRCYe can be used to also forecast yield before the end of the season. In this mode, VeRCYe was modified to use only the highest 50%, 40%, 30%, and 20% of the season's remotely sensed LAI data, as shown in Fig. 5, and was evaluated only at the field level. The period covered by this range of LAI percentage was recognized once the season's peak LAI was identified by using the concept of equivalent ratios. It is important to note that in this theoretical experimentation, APSIM simulations were generated from weather data recorded up to harvest. For this stage, only the RS LAI based on the RDVI was used, since it resulted in the best yield estimation accuracy while comparing the performance of the generic and adjusted LAI as inputs to VeRCYe. The objective here was also to see if the size of the LAI time series could be minimized and if so by how much, to save computation time and memory space while running the analysis. As a preliminary evaluation of the forecasting capabilities, this study used the same observed weather data in both modes.

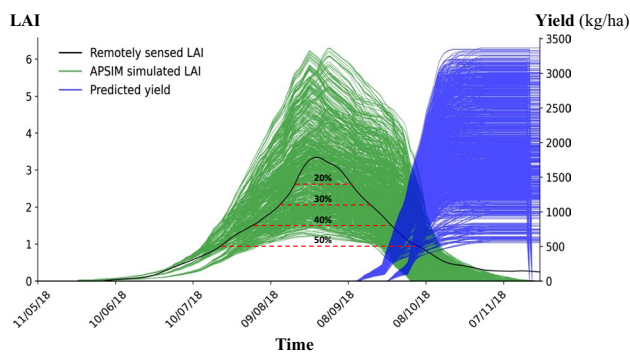


Fig. 5 Illustration of the periods covered by the highest 50%, 40%, 30%, and 20% of the season's remotely sensed Leaf Area Index (RS LAI) data. The RS LAI in black and the dashed red lines illustrate the field's highest percentage of the RS LAI values during the growing season.

2.5 Generating yield maps at the pixel level

VeRCYe estimates yield at the pixel level by converting the 3 m daily LAI maps produced from the fusion between PS and S2 (Sadeh et al. 2021). In this process, a Conversion Factor was used to convert LAI maps to yield maps (kg/ha). The Conversion Factor in our methodology serves as the bridge from this singular yield estimate, as derived from the APSIM simulation, to a more comprehensive yield map such that:

$$\text{Conversion Factor} = \frac{\text{Estimated yield}}{\text{Remotely sensed LAI}_{\max}}, \quad (2)$$

$$\text{Yield map} = \text{LAI map} \times \text{Conversion Factor}, \quad (3)$$

where estimated yield is the estimated field-scale yield and the remotely sensed LAI_{\max} corresponds to the season's maximum field-scale median LAI value from the RS LAI map, for the day on which RS LAI was detected as being the maximum within that field during the growing season. Next, using Eq. 3, each pixel of the LAI map was multiplied by the Conversion Factor, which converted the LAI values into yield (kg/ha) at the pixel level. This process resulted in a yield map at a spatial resolution of 3 m.

The accuracy of these yield maps was assessed using yield data collected by combine harvesters equipped with on-board yield monitors, which collected geolocated point yield data during the harvest. In this study, the harvesters' raw point measurements (commonly provided at a density of 10 m) were interpolated to a grid using the inverse distance weighting (IDW) interpolation (Bartier and Keller 1996) into standardized 5 m yield maps, after removing outlier measurements of less than 100 kg/ha or above 10,000 kg/ha, as well as data points located within 5 m of the field boundaries. Finally, the generated yield maps were smoothed by using a low pass filter (3×3 pixels kernel).

2.6 Harvest date detection

While forecasting yield is an important and challenging task, this study also identified when the crop is harvested and the predicted yield was ready to be transported from the farm for trading in the market. Consequently, the sowing detection method of Sadeh et al. (2019) was applied to harvest detection using PlanetScope imagery. It was found that the sowing detection method was effective in detecting the harvested area of the field, after modifying the "change" equation (Eq. 1) to

$$\text{Change} = \text{Image}_{t_1}^{\text{PC}_1} - \text{Image}_{t_2}^{\text{PC}_1}, \quad (4)$$

where the $\text{Image}_{t_2}^{\text{PC}_1}$ is the first principal component of the later image in the time series and $\text{Image}_{t_1}^{\text{PC}_1}$ is the first principal component of the earlier image. This modification was required, as sowing often corresponds to a change in color from bright to dark, while at harvest, the field changes from dark to bright.

3 Results

3.1 Sowing date detection accuracy

Implementing the sowing date detection method proposed by Sadeh et al. (2019) resulted in the accurate detection of sowing in 20 out of the 22 (90.9%) fields analyzed. For the fields that were successfully detected, there was an average gap of only 0.95-day (0.5-day gap for the median) between the detected and reported sowing dates (RMSE = 2.7 days).

3.2 Field-scale yield estimation accuracy

The results, as shown in Table 2, indicate that when using the fused LAI equivalent to the original generic S2-LAI, VeRCYe was able to estimate field-scale yield with a RMSE of 971 kg/ha (relative RMSE 39%) and an average and median error of -740 kg/ha and -573 kg/ha, respectively (for the best performing VI). The R^2 between the yield estimates using this dataset and the reported yield ranged between 0.84 and 0.89 for all VIs tested, while overall, the Modified Triangular Vegetation Index 2 (MTVI2)-based fused LAI outperformed the other VIs for most of the performance metrics. Using the adjusted LAI

improved the accuracy of the field-scale yield estimation substantially, with a RMSE of 757 kg/ha (relative RMSE 30%) and an average and median error of -519 kg/ha and -438 kg/ha, respectively (for the best performing VI). The best performing VI fusion-based LAI for the original LAI was MTVI2, and for the adjusted LAI, Renormalized Difference Vegetation Index (RDVI) was found to achieve the best accuracy. These two VIs were reported by Sadeh et al. (2021) to be among the best performing VIs to estimate wheat Green LAI using their proposed fusion method.

The R^2 between the estimated and reported yield ranged between 0.83 and 0.88 for all VIs tested, while overall, the RDVI-based fused LAI outperformed the other VIs for most of the performance metrics. Overall, this study found that VeRCYe was not very sensitive to the VI used to generate the fused LAI, as shown in Table 2. However, overall, the results highlight that using the fused LAI equivalent to the original generic S2-LAI underperformed for the field-scale yield predictions, resulting from using the adjusted LAI dataset. This study found that the adjusted RS LAI based on the RDVI resulted in the best yield prediction accuracy with $R^2 = 0.88$ and RMSE = 757 kg/ha (average of -15%) between the reported and estimated yield (Fig. 6). In addition, this method was able to estimate both the lowest (under 500 kg/ha) and highest yields (above 6500 kg/ha) with satisfactory accuracy, having an RMSE = 178 kg/ha (average error = 1 kg/ha, -1%) and 522 kg/ha (average error = 468 kg/ha, -7%), respectively. Despite these satisfactory results, VeRCYe tended to underestimate the reported yield in the tested conditions, as shown in Fig. 6.

Table 2 Performance of VeRSatellite Crop Yield Estimator (VeRCYe) field-scale yield estimations ($n = 27$) using either (i) the fused-based Leaf Area Index (LAI) dataset equivalent to the generic Sentinel-2 (S2) LAI (original) or (ii) the adjusted fused-based LAI that correct for underestimation of high LAI values (LAI > 3). This table shows

which of the 13 different vegetation indices (VI's) used in Sadeh et al. (2021) to fuse PS and S2 into high spatiotemporal resolution LAI resulted with the most accurate yield estimation. The best performances in each performance metric are highlighted in bold.

VI	NDVI	EVI2	MTVI2	MSAVI	WDRVI	Green WDRVI	GCVI	OSAVI	GSR	GNDVI	RDVI	TVI	SR
Original LAI													
Average error (kg/ha)	-845	-856	-740	-807	-847	-833	-827	-851	-826	-835	-774	-819	-835
Median error (kg/ha)	-868	-868	-573	-573	-868	-898	-870	-868	-870	-868	-653	-675	-833
RMSE (kg/ha)	1049	1059	971	1031	1044	1006	993	1053	993	1017	1002	1025	1038
Relative RMSE (%)	42	42	39	41	42	40	40	42	40	41	40	41	41
R^2	0.85	0.85	0.85	0.84	0.86	0.88	0.89	0.85	0.89	0.87	0.84	0.86	0.86
Adjusted LAI													
Average error (kg/ha)	-545	-558	-550	-572	-594	-563	-561	-538	-575	-556	-519	-579	-627
Median error (kg/ha)	-378	-378	-511	-488	-488	-525	-380	-378	-488	-525	-438	-488	-554
RMSE (kg/ha)	817	850	817	834	887	845	854	809	866	832	757	829	913
Relative RMSE (%)	33	34	33	33	35	34	34	32	35	33	30	33	36
R^2	0.86	0.84	0.86	0.86	0.83	0.85	0.84	0.86	0.84	0.85	0.88	0.86	0.83

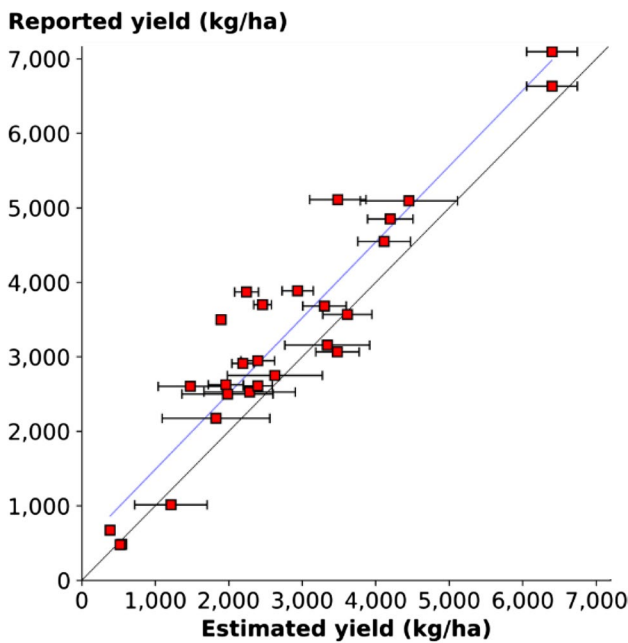


Fig. 6 Comparison between wheat yield reported by farmers and that estimated at the field scale by VeRsatile Crop Yield Estimator (VeRCYe), when using the adjusted RS LAI based on the RDVI. Each red square represents one of the 27 fields for which yield was reported by farmers; the whiskers represent the standard deviation of the estimated yield; the black line represents the 1:1 line; and the blue line represents the trend line. The accuracy analysis resulted in median error = -438 kg/ha, RMSE = 757 kg/ha, and $R^2 = 0.88$.

3.3 Yield map accuracy

The ability of VeRCYe to estimate yield at the pixel level was tested for 22 fields. The results, as shown in Table 3, indicate that when using the fused LAI, which was equivalent to the original generic S2-LAI, the proposed yield

estimation method was able to produce estimated yield maps with an RMSE of 1108 kg/ha and an average and median error of -467 kg/ha and -534 kg/ha, respectively (for the best performing VIs), at the pixel level (for all pixels of all maps). The R^2 between the yield estimates using this dataset and the reported yield ranged between 0.28 and 0.32 for all VIs tested, while overall the RDVI-based fused LAI slightly outperformed the other VIs.

In contrast to the improvement achieved by using the adjusted LAI dataset in estimating field-scale yield, using it to generate yield maps did not result in improved accuracy. Using the adjusted LAI resulted in an RMSE of 1213 kg/ha and an average and median error of -668 kg/ha and -819 kg/ha, respectively (for the best performing VIs), at the pixel level. The R^2 between the estimated yield maps and the harvesters' yield maps ranged between 0.27 and 0.32 on average for all VIs tested, while overall, the RDVI and the GSR-based fused LAI outperformed the other VIs in most of the parameters. It is important to note that in some cases the correlation at the pixel level between the harvester and the estimated yield maps was higher than $R^2 = 0.81$ (RMSE > 525 kg/ha) as shown in Fig. 7.

3.3.1 Sowing dates as model inputs

The result of the analysis shows a significant improvement in the accuracy of the yield estimation when using the detected sowing dates as inputs to the model instead of a rule-based sowing window. As shown in Fig. 8, using the sowing window with the adjusted fused-based LAI, the R^2 and RMSE between the reported and estimated yield were 0.71 and 1271 kg/ha, respectively, while using the detected sowing dates resulted in $R^2 = 0.88$ and RMSE of 757 kg/ha.

Table 3 The performance of VeRsatile Crop Yield Estimator (VeRCYe) to accurately generate sub-field-scale yield estimation by creating 3 m yield maps ($n = 22$). This table shows a comparison of the accuracy of the yield maps from either (i) the fused-based Leaf Area Index (LAI) dataset equivalent to the generic Sentinel-2 (S2)

LAI (original) or (ii) the adjusted fused-based LAI. This table shows which of the 13 different vegetation indices (VI's) tested by Sadeh et al. (2021) to fused PS and S2 into high spatiotemporal resolution LAI, resulted in the most accurate yield map estimation. The best performance in each metric is highlighted in bold.

VI	NDVI	EVI2	MTVI2	MSAVI	WDRVI	Green WDRVI	GCVI	OSAVI	GSR	GNDVI	RDVI	TVI	SR
Original LAI													
Average error (kg/ha)	-604	-625	-572	-652	-665	-644	-606	-605	-605	-660	-467	-660	-652
Median error (kg/ha)	-627	-607	-677	-681	-690	-646	-600	-627	-601	-654	-534	-683	-672
RMSE (kg/ha)	1108	1133	1215	1145	1184	1165	1148	1109	1147	1156	1199	1146	1183
R^2	0.30	0.31	0.28	0.30	0.32	0.31	0.32	0.30	0.32	0.31	0.30	0.30	0.32
Adjusted LAI													
Average error (kg/ha)	-894	-911	-687	-839	-886	-845	-813	-895	-812	-872	-668	-852	-856
Median error (kg/ha)	-999	-999	-855	-845	-966	-944	-926	-999	-927	-966	-819	-851	-976
RMSE (kg/ha)	1288	1303	1281	1258	1285	1235	1214	1289	1213	1250	1299	1261	1272
R^2	0.30	0.31	0.27	0.29	0.32	0.31	0.32	0.30	0.32	0.31	0.30	0.30	0.32

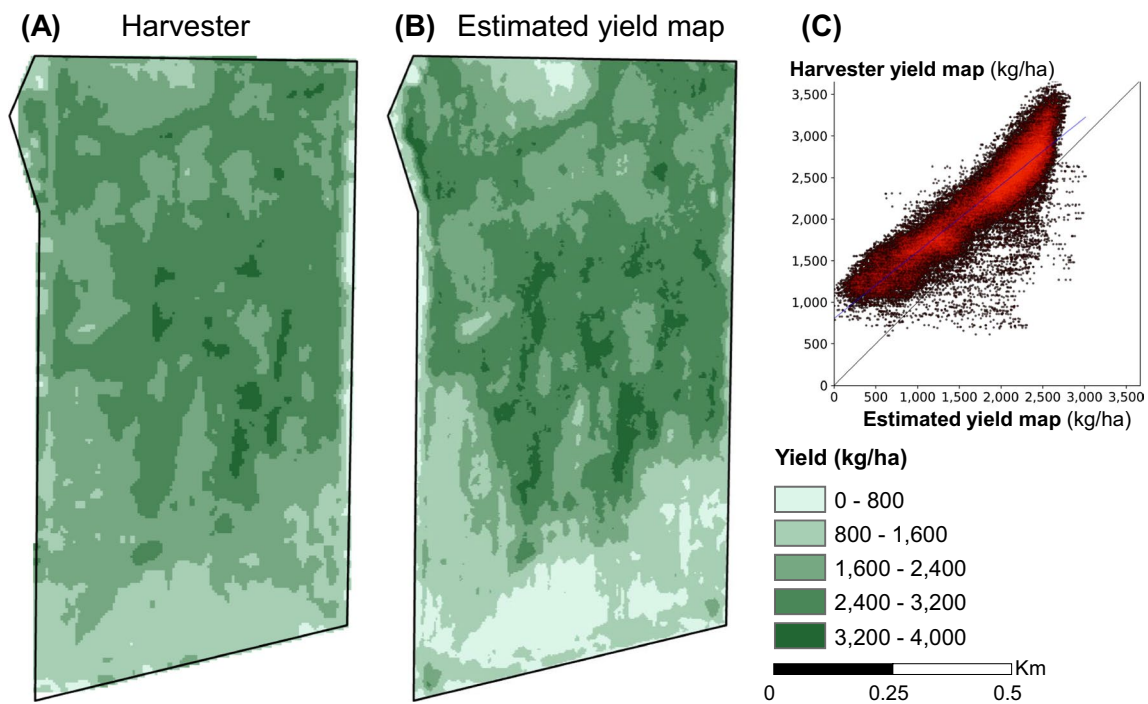


Fig. 7 Yield map produced by the combine harvester (A) and a yield map produced using the proposed methodology (B) and their comparison (C) for a wheat field located near Birchip, Victoria, Australia. **B** The estimated 3 m pixel size yield map. **C** The correlation between

the two yield maps is presented in the form of a scatterplot, where the black line signifies the 1:1 line and the blue line signifies the trend line. The correlation analysis between these maps found a RMSE = 525 kg/ha and $R^2 = 0.81$.

3.3.2 Yield forecasting using VeRCYe

In contrast to using the whole LAI time series of the growing season, this study also tested if VeRCYe has the potential to be used for yield forecasting rather than estimating and mapping the yield at the end of the growing season. Accordingly, VeRCYe was modified to use only the highest 50%, 40%, 30%, and 20% of the season's remotely sensed LAI data, as shown in Fig. 5.

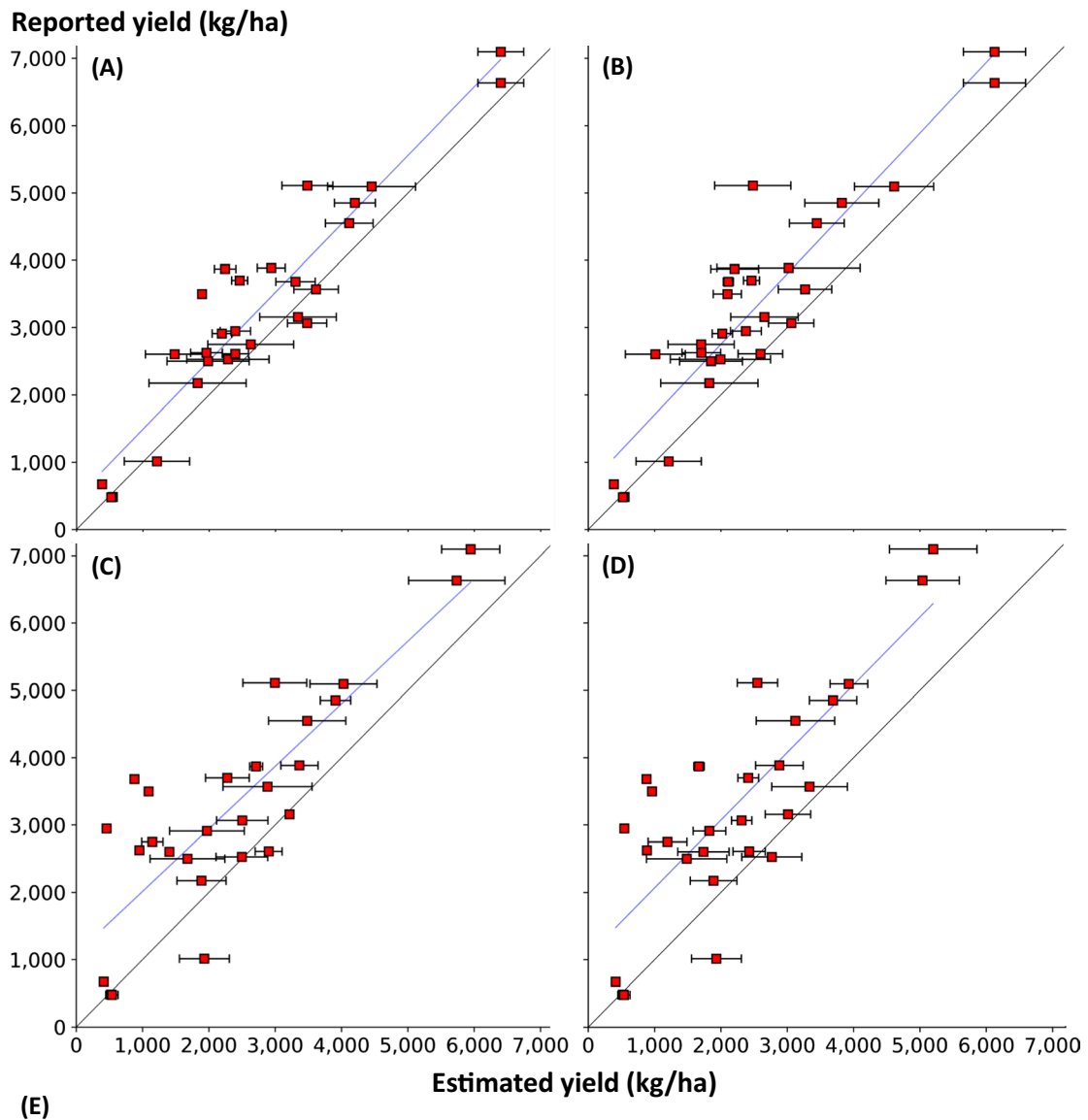
The results of the analysis show that even when using 50% or less of the RS LAI dataset (Fig. 9), VeRCYe was able to forecast the final yield ($R^2 = 0.88$ – 0.78) from about 2 months before the harvest (Fig. 10), while slightly underperforming the yield estimation made using the full RS LAI data (Fig. 6). However, as shown in Fig. 9, the shorter the time period used, the lower the accuracy. In addition, when comparing the forecasted yield by using both the generic and adjusted LAI as inputs to VeRCYe, using the adjusted LAI led to better accuracy in most cases, except for the R^2 (Fig. 9). Figure 10 shows how long before the harvest the yield could be forecast and the duration of the period that LAI was monitored to enable that forecast (more than a month after the LAI peak for 50% of the data and less than 3 weeks after the peak for 20% of the LAI dataset).

The findings of this study underscore the significance of segmenting the LAI dataset into two distinct components:

Green LAI and Senescence-LAI. This segmentation is crucial for enhancing the accuracy of yield forecasts (Fig. 9). When the LAI dataset is analyzed over a shorter temporal span, the critical distinctions between Green LAI and Senescence-LAI become less pronounced, leading to a decrease in the precision of the resultant field forecasts.

3.3.3 Harvest date detection

This study identified and mapped harvested area over the studied fields, by applying the sowing detection method proposed by Sadeh et al. (2019). All 20 analyzed fields had their harvest date detected with an average -0.1 -day gap (0-day gap for the median) between the detected and the reported harvest dates (RMSE = 2.6 days). The results show that after making small adjustments for harvest detection, the method was also suitable for detecting harvested area and its timing (Fig. 11). As illustrated in Fig. 11(A), the pre-harvested wheat can be seen in a dark brown color, while the harvested area has bright yellow/gray colors. Figure 11(B) shows the images resulting from subtracting $\text{Image}_{t_1}^{\text{PC}_1}$ from $\text{Image}_{t_2}^{\text{PC}_1}$, where a change between the images resulted in high values (green) and insignificant changes resulted in low values (red). The area classified as harvested is shown in white (Fig. 11(C)), and the gray areas are classified as noise.

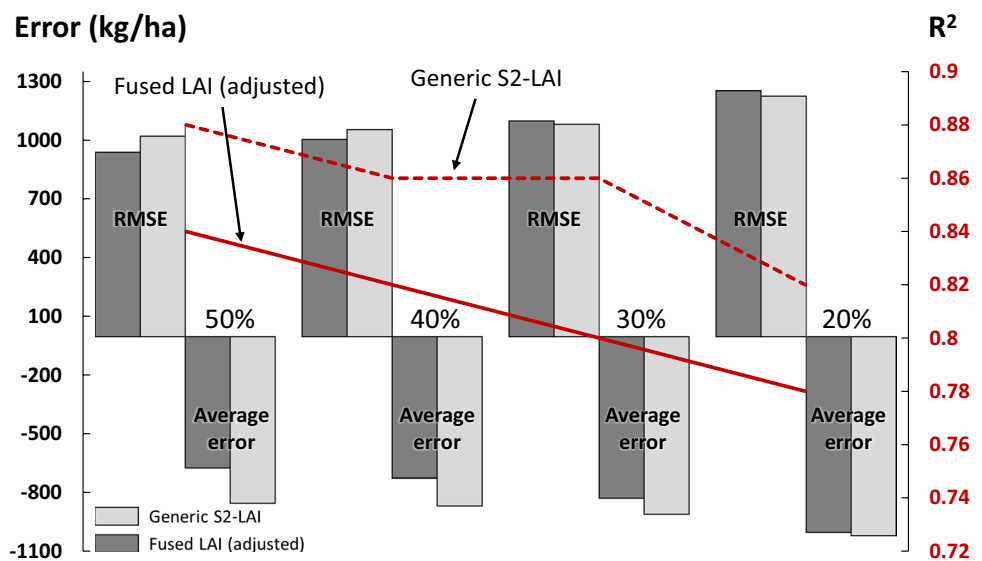


	(A) Detected sowing date & Adjusted LAI	(B) Detected sowing date & Non-adjusted LAI	(C) Sowing window & Adjusted LAI	(D) Sowing window & Non-adjusted LAI
Average error	-519	-774	-918	-1,073
Median error	-438	-653	-944	-1,089
RMSE (kg/ha)	757	1,002	1,271	1,431
R ²	0.88	0.84	0.71	0.65

Fig. 8 Comparison between the accuracy of the VeRsatile Crop Yield Estimator (VeRCYe) yield estimations when using the detected sowing dates for each field and its accuracy when a rule-based sowing window was used to determine the fields’ sowing dates for APSIM simulations. **A** The outcome of VeRCYe using the adjusted fused-based Leaf Area Index (LAI) with the detected sowing dates, **B** the

fused-based LAI dataset equivalent to the generic Sentinel-2 (S2)-LAI (original) with the detected sowing dates, **C** the adjusted fused-based LAI with a sowing window, **D** the fused-based generic S2-LAI with a sowing window, and **E** statistical summary of the analysis is presented in the table at the bottom of the figure.

Fig. 9 Results of using VeR-satellite Crop Yield Estimator (VeRCYe) in forecasting mode when using only the highest 50%, 40%, 30%, or 20% of the season's remotely sensed (RS) Leaf Area Index (LAI) data. This figure shows the outcome of yield forecasting at a field scale from using the generic and adjusted LAI datasets, by examining their RMSE and average error in kg/ha (gray columns) and R^2 (red lines).



4 Discussion

4.1 Wheat yield estimation at the field scale

Despite extensive research on remotely sensed yield estimation, it remains difficult to directly compare the results of this study with other studies on field-scale yield estimation, mainly owing to the lack of similarity in crop type, geographical location, and time frame of these estimations (Dado et al. 2020). However, this study demonstrated the capacity of VeRCYe both to predict and to map wheat yield prior to harvest with satisfactory accuracy, along with its potential in yield forecasting months before the harvest. The results suggest that using wheat-adjusted LAI (Sadeh et al. 2021) improves the accuracy of field-scale yield estimates substantially in comparison to using the fused LAI, which is equivalent to the original generic S2-LAI.

VeRCYe was found to provide a scalable approach for estimating wheat yield without the need for calibration, performing almost as well (and sometimes even better) than approaches that use field data for calibration (e.g., Feng et al. 2020; Donohue et al. 2018; Filippi et al. 2019; Zhao et al. 2020; Cai et al. 2019; Chen et al. 2020); all of these studies required the collection of an extensive and unique dataset measured *in situ* to train or calibrate their models. These datasets are rare, expensive to obtain, and very time consuming to perform. Furthermore, these methods, which require calibration through ground data, are typically limited in applicability to the areas from which the ground data were obtained. In addition, most methods provide yield estimates at a low resolution and often cannot be used for field and sub-field-scale yield predictions. One of the reasons why many of these studies have estimated yield at the regional scale is the difficulty to predict yield at a smaller scale, owing to variability of the environmental conditions

Fig. 10 Outcomes of the yield forecasting at a field scale from using the generic (light-gray) and adjusted (dark-gray) Leaf Area Index (LAI) datasets. Sub-figure (A) shows how long before the harvest the yield could be forecasted and sub-figure (B) the length of the period needed to be monitored after the peak of the season's LAI for each of the highest 50%, 40%, 30%, or 20% of the season's remotely sensed (RS) LAI data.

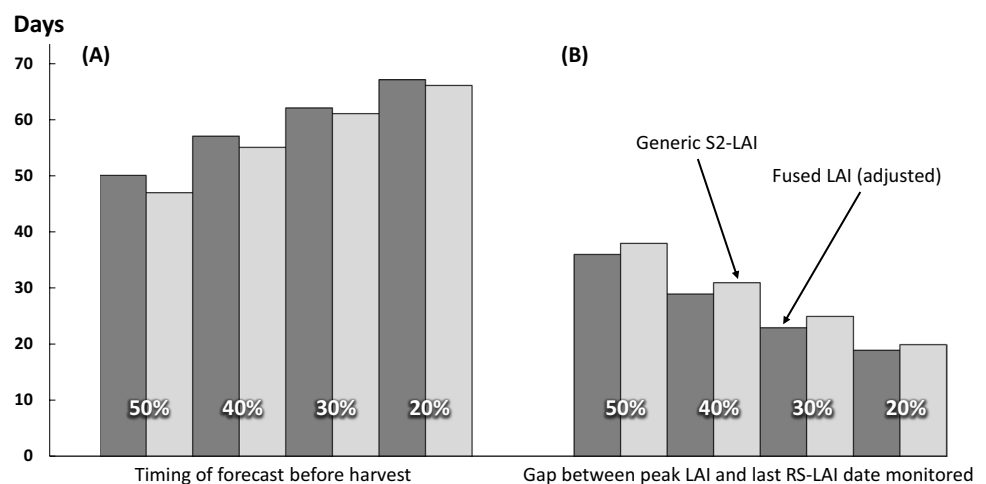
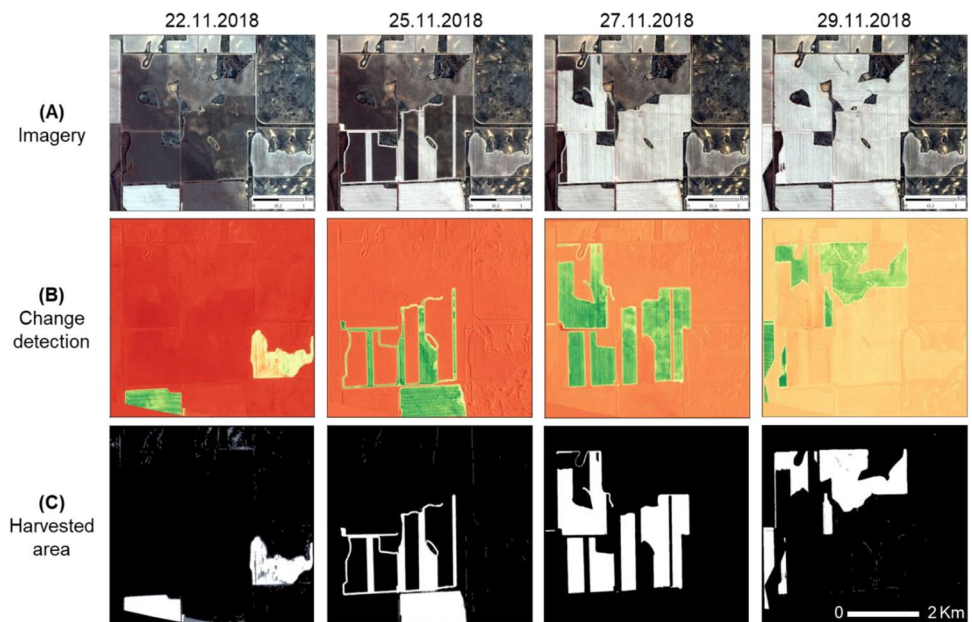


Fig. 11 Example of harvest detection. This figure illustrates the harvest detection of a 1400-ha farm near Mullewa, Western Australia, using four Planet-Scope images taken over 8 days. Refer to the text for details.



and farm practices, even within the same region (Feng et al. 2020). The development of VeRCYe was motivated to overcome these limitations, with its great advantage being that it uses agro-physiological knowledge embedded in a crop model (APSIM), which can be directly related to crop performance monitored by a satellite through time and space. In addition, VeRCYe can theoretically be applied to different crop types across different regions, without the need for local calibration, while being applicable for a rapidly changing environment (e.g., Ababaei and Chenu 2020; Collins and Chenu 2021) to which farmers are already adapting (e.g., Flohr et al. 2018).

The SCYM approach (Lobell et al. 2015), which offers yield estimation at the pixel level and employs regression methods to relate satellite imagery to gridded meteorological data, had some promising results when first tested in estimating yield at the field-scale for maize ($R^2 = 0.35$) and soybean ($R^2 = 0.32$) in the Midwestern United States (Lobell et al. 2015). However, later studies that tested the method for wheat yield estimation achieved limited success. Despite several attempts to use SCYM for wheat yield estimation with a range of different satellites having different temporal and spatial resolutions (Azzari et al. 2017; Jain et al. 2017; e.g., Jain et al. 2016; Shen and Evans 2021; Campolo et al. 2021), none of these attempts resulted in better performance than the proposed VeRCYe approach, as demonstrated in this study.

Globally, agriculture is critical to the livelihoods of millions of people, with low-yield harvests being directly correlated to high levels of food insecurity (Becker-Reshef et al. 2020). Therefore, when crop conditions are extremely poor, yield forecasting methods require these failures to be flagged early. Methods that use ground-based data for calibration

and training of their models (such as those using machine learning techniques) typically do not have the required ground reference data to represent the yield heterogeneity of the region of interest over space and time (Benami et al. 2021). Not having training data that reflects extremely low-yield scenarios may prevent these methods from producing accurate and reliable yield estimates. Conversely, VeRCYe managed to estimate such extremely low-yield fields (Fig. 6), despite being tested over wheat fields heavily impacted by one of the worst droughts in Australia in the last decade (Tian et al. 2019). This was achieved by identifying a field-scale failure, which was determined as a worst-case scenario.

Despite its popularity, the use of the peak LAI to estimate yield is likely to achieve poor predictions (Waldner et al. 2019). LAI by itself is limited as a linear indicator for the crop's yield, as this may be due to failure of plant development, or biotic or abiotic stresses (Huang et al. 2019; Benami et al. 2021). That also applies for the limited linear relationship between the VIs peak and the final yield (Kamir et al. 2020). However, it has been indicated by Dado et al. (2020) that using the peak of the Green Chlorophyll Vegetation Index (GCVI) and a window of 30 days after the peak allowed a slightly better yield estimation to be achieved than using the GCVI peak alone. Similarly, the current study indicates that the wider the window, the more accurate the yield estimation (Fig. 9 and 10). Accordingly, this study also highlights the need to watch the Senescence-LAI, owing to its important role in grain development. Figure 3 shows that while the simulated LAI peaks from different combinations of possible scenarios may be similar in timing and magnitude, only during the Senescence-LAI could the full pattern that better represented the final yield be identified. As optical remote sensing largely represents the Green

LAI (Haboudane et al. 2004), identifying an identical pattern between the simulated and RS LAI over the entire time series very likely results in an underestimation of the final yield. Therefore, VeRCYe includes a step which divides the RS LAI series into two, Green LAI and Senescence-LAI, and analyzes each separately.

In addition, the agreement between APSIM simulated LAI values and the remotely sensed LAI is not perfect (Waldner et al. 2019), even without the imbedded noise in the satellite data (Sadeh et al. 2021). For example, Ahmed et al. (2016) reported that APSIM leans slightly towards the overestimation of LAI. The observed discrepancy found in this study may be attributable to either inaccuracies in the remotely sensed LAI or potential limitations within the crop mode. Consequently, future research should strive to ascertain the origin of this error and examine its implications for methodologies that aim to integrate remote sensing data with crop modeling.

4.2 Yield maps at the pixel scale

Yield maps can help with estimating profitability, assessing the impacts of treatments used, establishing management zones, estimating the amount of nutrients removed by the harvested crop, improving farmers' skills, reducing yield gaps, and identifying areas that have predominantly large continuous gaps (Fulton et al. 2018; Lobell et al. 2015; Zhao et al. 2020). However, to reduce yield gaps (the difference between achievable yield and the actual yield), accurate yield estimates and their magnitude are needed, which represents their spatial and temporal variability (Hochman et al. 2012). The 3 m yield maps produced by VeRCYe can help to address these challenges, especially in regions where reliable geolocated yield data obtained from harvesters is not available, such as in many developing countries.

The accuracy of the yield maps generated by VeRCYe resulted in $R^2 = 0.32$ (RMSE of 1213 kg/ha) using the best-performing VI (RDVI). These results are equivalent to the accuracy of other yield mapping methods reported in the literature (e.g. Manivasagam et al. 2021; Sagan et al. 2021; Kamir et al. 2020; Dado et al. 2020). However, unlike VeRCYe, the methods used in these studies require local calibration, which limits their ability to estimate crop yield over large areas or in different environments from where the calibration data was gathered.

The SCYM (Lobell et al. 2015), which is similar to VeRCYe, can theoretically be applied anywhere in the world and produce a yield map at the pixel scale. While a pixel-by-pixel comparison of SCYM against harvester-based yield monitor data showed similar results, these studies looked at crop types other than wheat. For example, for maize,

Jeffries et al. (2019) reported R^2 average value of 0.12 and Deines et al. (2021) reported $R^2 = 0.31$ –0.4, and for soybean, Dado et al. (2020) reported $R^2 = 0.27$. Waldner et al. (2019) suggested that the temporal resolution is more important than the spatial resolution for accurate yield estimation, and therefore, the accuracy reported in this study may have been achieved owing to the high-temporal resolution (daily) of the dataset rather than its high-spatial resolution (3 m).

The comparative lower accuracy of the yield map estimated by our method relative to the yield map generated from the combine harvester can be attributed to several factors. One potential source of this discrepancy is the positional accuracy of the sensors, which is reported to have a RMSE of less than 10 m (Planet Team 2018). Additionally, the absence of a co-registration component in the fusion process may contribute to this inaccuracy. More significantly, however, the reduced accuracy appears to be a consequence of the method used to convert LAI pixel data into yield estimates, facilitated by the Conversion Factor. In its present implementation, the Conversion Factor effectuates a linear transformation from LAI to yield. This linear approach may not be entirely representative, considering that the relationship between LAI and yield is not strictly linear. As a result, this linear conversion is likely to lead to underestimation of yield in high-yielding portions of the field and overestimation in areas of lower yield. Therefore, it is crucial for future research to explore alternative formulations of the Conversion Factor concept, potentially adopting non-linear models that more accurately reflect the complex relationship between LAI and yield.

4.3 Sowing dates as model inputs

Sowing dates are an important input for crop models; therefore, obtaining accurate farm and regional scale information about the date when a crop was sown can assist in improving the reliability of crop simulations (Chenu et al. 2017; Holzworth et al. 2014; Flohr et al. 2017; Zheng et al. 2018; Mathison et al. 2017). Not knowing that parameter may result in a failure in capturing the full yield variation present within that region (Deines et al. 2021). Therefore, instead of using officially reported sowing dates (e.g., Marinho et al. 2014; Jin et al. 2016; Sakamoto et al. 2005) or a sowing date window (e.g., Azzari et al. 2017; Lobell et al. 2015), this study used the actual detected sowing dates as model inputs.

This study showed that when using the detected sowing dates, VeRCYe's yield estimation accuracy was substantially higher than using a rule-based sowing window (Fig. 8). While this is true when using VeRCYe at the field scale, future studies should explore the benefit of detecting the sowing date for each individual field when implementing VeRCYe at a regional scale.

4.4 Yield forecasting using VeRCYe

This study showed that VeRCYe can be very useful in estimating and mapping wheat yield at the end of the growing season without a requirement for local calibration, which has many applications. However, producing reliable forecasts of yield as far as possible ahead of harvest is important for food security monitoring, commodity traders, governments, and market stability (Benami et al. 2021; Becker-Reshef et al. 2020; Hammer et al. 2001). Hence, a method that is able to provide reliable wheat yield forecasting through space and time is needed.

The current study tested VeRCYe's potential in the forecasting mode, which uses only a part of the LAI data (Fig. 5), theoretically enabling it to forecast the yield about 2 months before the harvest (Fig. 10). The results show a moderate decline in the accuracy of the forecasted yield when a shorter LAI window around the peak of the LAI is used. Future studies should examine VeRCYe's performance when the field's LAI is being monitored from the beginning of the season up to three weeks after the peak, which according to Fig. 10 would allow to forecast yield more than 2 months before the harvest.

This study noted that computation wise, there is not much of a difference when running VeRCYe, at the field level, with the whole LAI time series of the growing season, or only the highest 50%, 40%, 30%, and 20% of the season's remotely sensed LAI data. However, it is likely that when running the proposed method on large scales, then the length of the period covered will affect the processing time.

4.5 Harvest date detection

The findings of this study underscore the efficacy of the tested change detection method in accurately identifying harvested wheat fields and tracking harvest progression both spatially and temporally. In this instance, the discernible contrast between senescing crops and the post-harvest residue was effectively utilized as an indicator of harvest completion. The technique developed by Sadeh et al. (2019) proved highly effective in detecting harvested fields across the Australian wheatbelt. However, there remains a need for further research to assess its applicability in different environmental contexts and to evaluate its performance at a larger scale. A critical factor contributing to the high accuracy of this study was the employment of PlanetScope's daily imagery. Nonetheless, it is important to note that in certain situations, the frequent presence of cloud cover may impede the use of such imagery. Consequently, it seems plausible to suggest that in other regions of the world, SAR-based change detection methods might be more appropriate for similar applications.

4.6 Limitations and prospects

Despite the results presented in this paper, there are some limitations and prospects that should be noted. The assumption that LAI and yields can be simulated accurately by crop models, such as APSIM, is the basis of VeRCYe. However, those models generally do not take biotic stress into consideration. In addition, they are also theoretic models and are thus imperfect by nature. Brown et al. (2018), who evaluated the APSIM-Wheat performance, found the model to estimate wheat yield with $R^2 = 0.84$ and $RMSE = 100.5$ kg/ha. While APSIM was used in this study, VeRCYe could be implemented using other process-based crop models that may be better adapted to other regions and/or crops. Future studies should evaluate its performance with other crop models.

VeRCYe uses the remotely sensed LAI_{max} (the day when RS LAI was detected as being the maximum during the growing season at the field level) to convert the LAI values into yield at the pixel level. However, this approach is not ideal, given that spatial differences in LAI may be due to different causes (e.g., different soil types, different topographies prone to flooding or frost, differences in water or nutrient availability), which are likely to impact differently the crop development and growth and ultimately the yield.

Yield estimation at the field-scale or its associated yield map (accurate as they can be) only provides information about yield, and the map itself cannot identify the yield-impacting factors. By contrast to most other yield estimation methods, VeRCYe identifies the best model simulations out of thousands of simulations that cover a representative range of on-farm management practices and possible environmental conditions. This enables the on-farm management practices used in the selected best-fit simulations to be extracted for investigation. For example, when analyzing field-scale yield over a specific region, the practices resulting in the highest or lowest yields can be identified, and the management practices that may help farmers to improve their productivity can be recommended. However, it is possible that the method produces accurate yield estimates for the wrong reasons. Having multiple changing parameters may end up with more knobs than can be turned, which can increase the chance of getting right-looking answers from an incorrect set of parameters. Therefore, further research is needed to verify if the optimal APSIM parameters actually reflect the conditions on the ground, which requires a very detailed record of farm management practices used by the farmers. However, such an analysis is beyond the scope of this study.

Importantly, VeRCYe was used here with APSIM simulations generated from weather data recorded up to harvest. In a full forecasting mode, forecasted weather data or historical weather data capturing climatic variability for the site should be used to evaluate the likely crop growth and development

of the remainder of the season. The process of selecting the best fit simulated LAI to the RS LAI should also be the focus of future studies, together with testing VeRCYe's ability to generate yield forecasts using forecasted weather data.

While the method proposed here was tested for the estimation of wheat yields, it is probable that it would also be capable of predicting yield for other crops. This can be done by running a suitable crop simulator (e.g., APSIM-Maize) and by adjusting the parameters listed in Table 1 to reflect the typical local practices for each crop. However, the results of this study indicate that adjustment of generic S2-LAI data for improving the estimates of the Green LAI, as proposed by Sadeh et al. (2021), is needed in order to achieve better yield estimation. Moreover, it is likely that such an adjustment will also be needed when implementing VeRCYe with other crop types.

While this method relies on the availability of LAI data from optical sensors, these are highly sensitive to the presence of clouds and shadows in the imagery, which is likely to limit the ability to perform at its best over certain regions. SAR sensors have the advantage over optical sensing of providing all-weather capability, and harnessing these offers the prospect of an improvement to VeRCYe should include the use of SAR-based LAI or SAR-optical fused LAI.

In the context of this study, the utilization of PlanetScope imagery proved as useful for generating high-resolution fused images and in accurately detecting sowing and harvest dates. However, it is critical to acknowledge that PlanetScope data is not freely available for commercial applications. This aspect necessitates further research to investigate the viability of alternative satellite imagery sources that are accessible to the public at no cost. Exploring these freely available options is essential for the broader applicability and sustainability of similar studies in commercial settings.

The advantage of being able to estimate field and farm productivity remotely without the need of having “boots on the ground” has been magnified by the outbreak of COVID-19. While lockdowns and prolonged COVID-19 quarantine measures delay/limit the supply of essential products, such as fertilizers, herbicides, machinery, or even the availability of seasonal workers, affecting the farmers' performance, it has also decreased feed wheat and wheat-based product demand (FAO 2021). VeRCYe can potentially help to monitor these influences remotely across different regions without the need to risk surveyors in collecting ground data.

The proposed method allows the crop performance to be monitored throughout the season, from their sowing dates until the farmer decides to harvest and the yield becomes available to be traded as a food product.

5 Conclusions

The main contribution of the VeRCYe method is that it overcomes the major limitation of previous studies, namely, the need for ground data in model building and calibration for estimating wheat yield. VeRCYe does so by leveraging the combined advantages of crop model simulations and high spatiotemporal resolution remote sensing. This approach allowed sowing date data required for model inputs to be estimated from satellite data. It also permits remotely sensed field- and pixel-scale estimation of crop yield without the need to compromise between high temporal resolution and high spatial resolution. Since VeRCYe is not dependent on ground calibration data, it offers broad applications across regions where ground calibration data are not available. Experiments to test the method showed it to be reliable for estimating field-scale wheat yields ($R^2 = 0.88$, RMSE = 757 kg/ha). Importantly, these experiments also revealed the potential of VeRCYe to produce 3 m resolution yield maps months before the wheat harvest ($R^2 = 0.32$, RMSE = 1213 kg/ha). Although the current study was conducted on wheat, the method may also be implemented to predict the yields of other crop types, with only minimum adaptation. This study thus outlined an innovative approach to monitor farm management practices at 3 m, from sowing, through monitoring the crop performance throughout the season, until harvest when the yield becomes available for trading as a food product. Furthermore, the information generated with this method can be used to understand yield variability from a regional scale to a pixel scale and may provide insights into the causes and spatial distribution of this variability.

Acknowledgements The authors would like to thank Planet Labs, Inc., for providing us with the PlanetScope imageries used in this study. Tim McClelland (Partner A.W. McClelland & Co, Birchip VIC 3483, Australia) for his support and for providing field-scale validation data.

Authors' contributions Conceptualization and methodology: Y.S. and K.C.; data analysis: Y.S., Y.C., and K.C.; supervision: X.Z., D.D., J.P.W., and K.C.; validation and data curation: D.D., J.P.W., Y.C., and K.C.; writing—original draft: Y.S.; and review and editing: X.Z., D.D., J.P.W., Y.C., and K.C. All authors read and approved the final manuscript.

Funding Open Access funding enabled and organized by CAUL and its Member Institutions. This work was supported by the Co-Funded Monash Graduate Scholarship awarded to Y. Sadeh by Monash University.

Data availability For privacy reasons, qualitative raw data will not be shared.

Code availability Not applicable.

Declarations

Ethics approval Not applicable.

Consent to participate Not applicable.

Consent for publication Not applicable.

Conflict of interest We wish to disclose that Dr. Karine Chenu, a co-author of this manuscript, also serves as an Editor on the journal, and was not involved in the evaluation process at any stage.

Open Access This article is licensed under a Creative Commons Attribution 4.0 International License, which permits use, sharing, adaptation, distribution and reproduction in any medium or format, as long as you give appropriate credit to the original author(s) and the source, provide a link to the Creative Commons licence, and indicate if changes were made. The images or other third party material in this article are included in the article's Creative Commons licence, unless indicated otherwise in a credit line to the material. If material is not included in the article's Creative Commons licence and your intended use is not permitted by statutory regulation or exceeds the permitted use, you will need to obtain permission directly from the copyright holder. To view a copy of this licence, visit <http://creativecommons.org/licenses/by/4.0/>.

References

- Ababaei B, Chenu K (2020) Heat shocks increasingly impede grain filling but have little effect on grain setting across the Australian wheatbelt. *Agric for Meteorol* 284:107889. <https://doi.org/10.1016/j.agrformet.2019.107889>
- Ahmed M, Akram MN, Asim M, Aslam M, Hassan FU, Higgins S, Stöckle CO, Hoogenboom G (2016) Calibration and validation of APSIM-Wheat and CERES-Wheat for spring wheat under rainfed conditions: models evaluation and application. *Comput Electron Agric* 123:384–401. <https://doi.org/10.1016/j.compag.2016.03.015>
- Amherdt S, Di Leo NC, Balbarani S, Pereira A, Cornero C, Pacino MC (2021) Exploiting Sentinel-1 data time-series for crop classification and harvest date detection. *Int J Remote Sens* 42(19):7313–7331. <https://doi.org/10.1080/01431161.2021.1957176>
- Azzari G, Jain M, Lobell DB (2017) Towards fine resolution global maps of crop yields: testing multiple methods and satellites in three countries. *Remote Sens Environ* 202:129–141. <https://doi.org/10.1016/j.rse.2017.04.014>
- Bartier PM, Keller CP (1996) Multivariate interpolation to incorporate thematic surface data using inverse distance weighting (IDW). *Comput Geosci* 22(7):795–799. [https://doi.org/10.1016/0098-3004\(96\)00021-0](https://doi.org/10.1016/0098-3004(96)00021-0)
- Becker-Reshef I, Vermote E, Lindeman M, Justice C (2010) A generalized regression-based model for forecasting winter wheat yields in Kansas and Ukraine using MODIS data. *Remote Sens Environ* 114(6):1312–1323. <https://doi.org/10.1016/j.rse.2010.01.010>
- Becker-Reshef I, Justice C, Barker B, Humber M, Rembold F, Bonifacio R, Zappacosta M, Budde M, Magadzire T, Shitote C, Pound J, Constantino A, Nakalembe C, Mwangi K, Sobue S, Newby T, Whitcraft A, Jarvis I, Verdin J (2020) Strengthening agricultural decisions in countries at risk of food insecurity: the GEOGLAM Crop Monitor for Early Warning. *Remote Sens Environ* 237:111553. <https://doi.org/10.1016/j.rse.2019.111553>
- Benami E, Jin ZN, Carter MR, Ghosh A, Hijmans RJ, Hobbs A, Kenduywo B, Lobell DB (2021) Uniting remote sensing, crop modelling and economics for agricultural risk management. *Nat Rev Earth Environ* 2(2):140–159. <https://doi.org/10.1038/s43017-020-00122-y>
- Beyene AN, Zeng HW, Wu BF, Zhu L, Gebremicael TG, Zhang M, Bezabh T (2022) Coupling remote sensing and crop growth model to estimate national wheat yield in Ethiopia. *Big Earth Data* 6(1):18–35. <https://doi.org/10.1080/20964471.2020.1837529>
- Bognár P, Kern A, Pásztor S, Lichtenberger J, Koronczay D, Ferencz C (2017) Yield estimation and forecasting for winter wheat in Hungary using time series of MODIS data. *Int J Remote Sens* 38(11):3394–3414. <https://doi.org/10.1080/01431161.2017.1295482>
- Brown H, Huth N, Holzworth D (2018) Crop model improvement in APSIM: using wheat as a case study. *Eur J Agron* 100:141–150. <https://doi.org/10.1016/j.eja.2018.02.002>
- Burke M, Lobell DB (2017) Satellite-based assessment of yield variation and its determinants in smallholder African systems. *Proc Natl Acad Sci* 114(9):2189–2194. <https://doi.org/10.1073/pnas.1616919114>
- Cai YP, Guan KY, Lobell D, Potgieter AB, Wang SW, Peng J, Xu TF, Asseng S, Zhang YG, You LZ, Peng B (2019) Integrating satellite and climate data to predict wheat yield in Australia using machine learning approaches. *Agric for Meteorol* 274:144–159. <https://doi.org/10.1016/j.agrformet.2019.03.010>
- Campolo J, Güereña D, Maharjan S, Lobell DB (2021) Evaluation of soil-dependent crop yield outcomes in Nepal using ground and satellite-based approaches. *Field Crops Res* 260:107987. <https://doi.org/10.1016/j.fcr.2020.107987>
- Chen Y, Donohue RJ, McVicar TR, Waldner F, Mata G, Ota N, Houshmandfar A, Dayal K, Lawes RA (2020) Nationwide crop yield estimation based on photosynthesis and meteorological stress indices. *Agric for Meteorol* 284:107872. <https://doi.org/10.1016/j.agrformet.2019.107872>
- Chenu K, Cooper M, Hammer GL, Mathews KL, Dreccer MF, Chapman SC (2011) Environment characterization as an aid to wheat improvement: interpreting genotype-environment interactions by modelling water-deficit patterns in North-Eastern Australia. *J Exp Bot* 62(6):1743–1755. <https://doi.org/10.1093/jxb/erq459>
- Chenu K, Deihimfard R, Chapman SC (2013) Large-scale characterization of drought pattern: a continent-wide modelling approach applied to the Australian wheatbelt—spatial and temporal trends. *New Phytol* 198(3):801–820. <https://doi.org/10.1111/nph.12192>
- Chenu K, Porter JR, Martre P, Basso B, Chapman SC, Ewert F, Bindi M, Asseng S (2017) Contribution of crop models to adaptation in wheat. *Trends Plant Sci* 22(6):472–490. <https://doi.org/10.1016/j.tplants.2017.02.003>
- Collins B, Chenu K (2021) Improving productivity of Australian wheat by adapting sowing date and genotype phenology to future climate. *Clim Risk Manag* 32:100300. <https://doi.org/10.1016/j.crm.2021.100300>
- Coventry DR, Reeves TG, Brooke HD, Cann DK (1993) Influence of genotype, sowing date, and seeding rate on wheat development and yield. *Aust J Exp Agric* 33(6):751–757. <https://doi.org/10.1071/Ea9930751>
- Dado WT, Deines JM, Patel R, Liang SZ, Lobell DB (2020) High-resolution soybean yield mapping across the US Midwest using subfield harvester data. *Remote Sens* 12(21):3471. <https://doi.org/10.3390/rs12213471>
- Daughtry CST, Gallo KP, Goward SN, Prince SD, Kustas WP (1992) Spectral estimates of absorbed radiation and phytomass production in corn and soybean canopies. *Remote Sens Environ* 39(2):141–152. [https://doi.org/10.1016/0034-4257\(92\)90132-4](https://doi.org/10.1016/0034-4257(92)90132-4)
- Deines JM, Patel R, Liang S-Z, Dado W, Lobell DB (2021) A million kernels of truth: insights into scalable satellite maize yield

- mapping and yield gap analysis from an extensive ground dataset in the US Corn Belt. *Remote Sens Environ* 253:112174. <https://doi.org/10.1016/j.rse.2020.112174>
- Delegido J, Verrelst J, Rivera JP, Ruiz-Verdú A, Moreno J (2015) Brown and green LAI mapping through spectral indices. *Int J Appl Earth Obs Geoinf* 35:350–358. <https://doi.org/10.1016/j.jag.2014.10.001>
- Dong J, Lu HB, Wang YW, Ye T, Yuan WP (2020) Estimating winter wheat yield based on a light use efficiency model and wheat variety data. *ISPRS J Photogramm Remote Sens* 160:18–32. <https://doi.org/10.1016/j.isprsjprs.2019.12.005>
- Donohue RJ, Lawes RA, Mata G, Gobbett D, Ouzman J (2018) Towards a national, remote-sensing-based model for predicting field-scale crop yield. *Field Crops Res* 227:79–90. <https://doi.org/10.1016/j.fcr.2018.08.005>
- FAO (2021) Monthly news report on grains (trans: Division FMA/T). MNR. Food and Agriculture Organization of The United Nations (FAO)
- Feng PY, Wang B, Liu DL, Waters C, Xiao DP, Shi LJ, Yu Q (2020) Dynamic wheat yield forecasts are improved by a hybrid approach using a biophysical model and machine learning technique. *Agric for Meteorol* 285:107922. <https://doi.org/10.1016/j.agrformet.2020.107922>
- Ferencz C, Bognár P, Lichtenberger J, Hamar D, Tarcsai G, Timár G, Molnár G, Pásztor S, Steinbach P, Székely B, Ferencz OE, Ferencz-Arkos I (2004) Crop yield estimation by satellite remote sensing. *Int J Remote Sens* 25(20):4113–4149. <https://doi.org/10.1080/01431160410001698870>
- Filippi P, Jones EJ, Wimalathunge NS, Somarathna PDSN, Pozza LE, Ugabaje SU, Jephcott TG, Paterson SE, Whelan BM, Bishop TFA (2019) An approach to forecast grain crop yield using multi-layered, multi-farm data sets and machine learning. *Precision Agric* 20(5):1015–1029. <https://doi.org/10.1007/s11119-018-09628-4>
- Flohr BM, Hunt JR, Kirkegaard JA, Evans JR (2017) Water and temperature stress define the optimal flowering period for wheat in south-eastern Australia. *Field Crops Res* 209:108–119. <https://doi.org/10.1016/j.fcr.2017.04.012>
- Flohr BM, Hunt JR, Kirkegaard JA, Evans JR, Trevaskis B, Zwart A, Swan A, Fletcher AL, Rheinheimer B (2018) Fast winter wheat phenology can stabilise flowering date and maximise grain yield in semi-arid Mediterranean and temperate environments. *Field Crops Res* 223:12–25. <https://doi.org/10.1016/j.fcr.2018.03.021>
- Franch B, Vermote EF, Becker-Reshef I, Claverie M, Huang J, Zhang J, Justice C, Sobrino JA (2015) Improving the timeliness of winter wheat production forecast in the United States of America, Ukraine and China using MODIS data and NCAR Growing Degree Day information. *Remote Sens Environ* 161:131–148. <https://doi.org/10.1016/j.rse.2015.02.014>
- Fulton J, Hawkins E, Taylor R, Franzen A (2018) Yield monitoring and mapping. *Precision Agric Basics* 63–77. <https://doi.org/10.2134/precisionagbasics.2016.0089>
- Gao F, Anderson MC, Kustas WP, Wang YJ (2012) Simple method for retrieving leaf area index from Landsat using MODIS leaf area index products as reference. *J Appl Remote Sens* 6(1):063554. <https://doi.org/10.1117/1.Jrs.6.063554>
- Gitelson AA, Viña A, Ciganda V, Rundquist DC, Arkebauer TJ (2005) Remote estimation of canopy chlorophyll content in crops -: art. no. L08403. *Geophys Res Lett* 32(8). <https://doi.org/10.1029/2005gl022688>
- Haboudane D, Miller JR, Pattey E, Zarco-Tejada PJ, Strachan IB (2004) Hyperspectral vegetation indices and novel algorithms for predicting green LAI of crop canopies: modeling and validation in the context of precision agriculture. *Remote Sens Environ* 90(3):337–352. <https://doi.org/10.1016/j.rse.2003.12.013>
- Hammer GL, Hansen JW, Phillips JG, Mjelde JW, Hill H, Love A, Potgieter A (2001) Advances in application of climate prediction in agriculture. *Agric Syst* 70(2–3):515–553. [https://doi.org/10.1016/S0308-521x\(01\)00058-0](https://doi.org/10.1016/S0308-521x(01)00058-0)
- Hochman Z, Gobbett D, Holzworth D, McClelland T, van Rees H, Marinoni O, Garcia JN, Horan H (2012) Quantifying yield gaps in rainfed cropping systems: a case study of wheat in Australia. *Field Crops Res* 136:85–96. <https://doi.org/10.1016/j.fcr.2012.07.008>
- Holzworth DP, Huth NI, Devoil PG, Zurcher EJ, Herrmann NI, McLean G, Chenu K, van Oosterom EJ, Snow V, Murphy C, Moore AD, Brown H, Whish JPM, Verrall S, Fainges J, Bell LW, Peake AS, Poulton PL, Hochman Z, Thorburn PJ, Gaydon DS, Dalgliesh NP, Rodriguez D, Cox H, Chapman S, Doherty A, Teixeira E, Sharp J, Cichota R, Vogeler I, Li FY, Wang EL, Hammer GL, Robertson MJ, Dimes JP, Whitbread AM, Hunt J, van Rees H, McClelland T, Carberry PS, Hargreaves JNG, MacLeod N, McDonald C, Harsdorf J, Wedgwood S, Keating BA (2014) APSIM - evolution towards a new generation of agricultural systems simulation. *Environ Model Software* 62:327–350. <https://doi.org/10.1016/j.envsoft.2014.07.009>
- Holzworth D, Huth NI, Fainges J, Brown H, Zurcher E, Cichota R, Verrall S, Herrmann NI, Zheng B, Snow V (2018) APSIM next generation: overcoming challenges in modernising a farming systems model. *Environ Model Software* 103:43–51. <https://doi.org/10.1016/j.envsoft.2018.02.002>
- Houborg R, McCabe MF (2016) High-resolution NDVI from planet's constellation of earth observing nano-satellites: a new data source for precision agriculture. *Remote Sens* 8(9). <https://doi.org/10.3390/rs8090768>
- Houborg R, McCabe MF (2018) A Cubesat enabled Spatio-Temporal Enhancement Method (CESTEM) utilizing Planet, Landsat and MODIS data. *Remote Sens Environ* 209:211–226. <https://doi.org/10.1016/j.rse.2018.02.067>
- Houser PR, De Lannoy GJM, Walker JP (2012) Hydrologic data assimilation. Approaches to managing disaster - assessing hazards, emergencies and disaster impacts:41-64. <https://doi.org/10.5772/11112>
- Huang JX, Ma HY, Su W, Zhang XD, Huang YB, Fan JL, Wu WB (2015) Jointly assimilating MODIS LAI and ET products into the SWAP model for winter wheat yield estimation. *Ieee J Selected Topics Appl Earth Observ Remote Sens* 8(8):4060–4071. <https://doi.org/10.1109/Jstars.2015.2403135>
- Huang JX, Gómez-Dans JL, Huang H, Ma HY, Wu QL, Lewis PE, Liang SL, Chen ZX, Xue JH, Wu YT, Zhao F, Wang J, Xie XH (2019) Assimilation of remote sensing into crop growth models: current status and perspectives. *Agric for Meteorol* 276:107609. <https://doi.org/10.1016/j.agrformet.2019.06.008>
- Idso SB, Jackson RD, Reginato RJ (1977) Remote-sensing of crop yields. *Science* 196(4285):19–25. <https://doi.org/10.1126/science.196.4285.19>
- Ines AVM, Das NN, Hansen JW, Njoku EG (2013) Assimilation of remotely sensed soil moisture and vegetation with a crop simulation model for maize yield prediction. *Remote Sens Environ* 138:149–164. <https://doi.org/10.1016/j.rse.2013.07.018>

- Jain M, Srivastava AK, Balwinder-Singh JRK, McDonald A, Royal K, Lisaius MC, Lobell DB (2016) Mapping smallholder wheat yields and sowing dates using micro-satellite data. *Remote Sens* 8(10):860–878. <https://doi.org/10.3390/rs8100860>
- Jain M, Singh B, Srivastava AAK, Malik RK, McDonald AJ, Lobell DB (2017) Using satellite data to identify the causes of and potential solutions for yield gaps in India's wheat belt. *Environ Res Lett* 12(9). <https://doi.org/10.1088/1748-9326/aa8228>
- Jeffries GR, Griffin TS, Fleisher DH, Naumova EN, Koch M, Wardlow BD (2019) Mapping sub-field maize yields in Nebraska, USA by combining remote sensing imagery, crop simulation models, and machine learning. *Precision Agric* 21(3):678–694. <https://doi.org/10.1007/s11119-019-09689-z>
- Jin N, Tao B, Ren W, Feng MC, Sun R, He L, Zhuang W, Yu Q (2016) Mapping irrigated and rainfed wheat areas using multi-temporal satellite data. *Remote Sens* 8(3):207. <https://doi.org/10.3390/rs8030207>
- Jin ZN, Azzari G, Burke M, Aston S, Lobell DB (2017a) Mapping smallholder yield heterogeneity at multiple scales in Eastern Africa. *Remote Sens* 9(9):931. <https://doi.org/10.3390/rs9090931>
- Jin ZN, Azzari G, Lobell DB (2017b) Improving the accuracy of satellite-based high-resolution yield estimation: a test of multiple scalable approaches. *Agric for Meteorol* 247:207–220. <https://doi.org/10.1016/j.agrformet.2017.08.001>
- Jin ZN, Azzari G, You C, Di Tommaso S, Aston S, Burke M, Lobell DB (2019) Smallholder maize area and yield mapping at national scales with Google Earth Engine. *Remote Sens Environ* 228:115–128. <https://doi.org/10.1016/j.rse.2019.04.016>
- Kamir E, Waldner F, Hochman Z (2020) Estimating wheat yields in Australia using climate records, satellite image time series and machine learning methods. *ISPRS J Photogramm Remote Sens* 160:124–135. <https://doi.org/10.1016/j.isprsjprs.2019.11.008>
- Labus MP, Nielsen GA, Lawrence RL, Engel R, Long DS (2002) Wheat yield estimates using multi-temporal NDVI satellite imagery. *Int J Remote Sens* 23(20):4169–4180. <https://doi.org/10.1080/01431160110107653>
- Lai YR, Pringle MJ, Kopittke PM, Menzies NW, Orton TG, Dang YP (2018) An empirical model for prediction of wheat yield, using time-integrated Landsat NDVI. *Int J Appl Earth Obs Geoinf* 72:99–108. <https://doi.org/10.1016/j.jag.2018.07.013>
- Lawes R, Chen C, Whish J, Meier E, Ouzman J, Gobbett D, Vadakattu G, Ota N, van Rees H (2021) Applying more nitrogen is not always sufficient to address dryland wheat yield gaps in Australia. *Field Crops Res* 262:108033. <https://doi.org/10.1016/j.fcr.2020.108033>
- Leach N, Coops NC, Obrknezev N (2019) Normalization method for multi-sensor high spatial and temporal resolution satellite imagery with radiometric inconsistencies. *Comput Electron Agric* 164:104893. <https://doi.org/10.1016/j.compag.2019.104893>
- Lobell DB (2013) The use of satellite data for crop yield gap analysis. *Field Crops Res* 143:56–64. <https://doi.org/10.1016/j.fcr.2012.08.008>
- Lobell DB, Thau D, Seifert C, Engle E, Little B (2015) A scalable satellite-based crop yield mapper. *Remote Sens Environ* 164:324–333. <https://doi.org/10.1016/j.rse.2015.04.021>
- Louis J, Debaecker V, Pflug B, Main-Knorn M, Bieniarz J, Mueller-Wilm U, Cadau E, Gascon F (2016) Sentinel-2 Sen2Cor: L2A processor for users. In: *Proceedings living planet symposium 2016, Prague, Czech Republic*. Spacebooks Online, pp 1–8
- Manivasagam VS, Sadeh Y, Kaplan G, Bonfil DJ, Rozenstein O (2021) Studying the feasibility of assimilating Sentinel-2 and PlanetScope imagery into the SAFY crop model to predict within-field wheat yield. *Remote Sens* 13(12):2395. <https://doi.org/10.3390/rs13122395>
- Marinho E, Vancutsem C, Fasbender D, Kayitakire F, Pini G, Pekel JF (2014) From remotely sensed vegetation onset to sowing dates: aggregating pixel-level detections into village-level sowing probabilities. *Remote Sens* 6(11):10947–10965. <https://doi.org/10.3390/rs61110947>
- Marshall M, Tu K, Brown J (2018) Optimizing a remote sensing production efficiency model for macro-scale GPP and yield estimation in agroecosystems. *Remote Sens Environ* 217:258–271. <https://doi.org/10.1016/j.rse.2018.08.001>
- Mathison C, Deva C, Falloon P, Challinor AJ (2017) Defining sowing and harvest dates based on the Asian Summer Monsoon. *Earth Syst Dyn Discuss* 1–39. <https://doi.org/10.5194/esd-2017-88>
- Moulin S, Bondeau A, Delecote R (1998) Combining agricultural crop models and satellite observations: from field to regional scales. *Int J Remote Sens* 19(6):1021–1036. <https://doi.org/10.1080/014311698215586>
- Nakalembe C, Becker-Reshef I, Bonifacio R, Hu GX, Humber ML, Justice CJ, Keniston J, Mwangi K, Rembold F, Shukla S, Urbano F, Whitcraft AK, Li YY, Zappacosta M, Jarvis I, Sanchez A (2021) A review of satellite-based global agricultural monitoring systems available for Africa. *Glob Food Security-Agric Policy Econ Environ* 29:100543. <https://doi.org/10.1016/j.gfs.2021.100543>
- Pan HZ, Chen ZX, de Wit A, Ren JQ (2019) Joint assimilation of leaf area index and soil moisture from Sentinel-1 and Sentinel-2 data into the WOFOST model for winter wheat yield estimation. *Sensors* 19(14):3161. <https://doi.org/10.3390/s19143161>
- Planet Team (2018) Planet imagery product specifications. Planet Labs Inc. https://www.planet.com/products/satellite-imagery/files/Planet_Combined_Imagery_Product_Specs_December2017.pdf. Accessed 12/04/2018 2018
- Prasad AK, Chai L, Singh RP, Kafatos M (2006) Crop yield estimation model for Iowa using remote sensing and surface parameters. *Int J Appl Earth Obs Geoinf* 8(1):26–33. <https://doi.org/10.1016/j.jag.2005.06.002>
- Prévoit L, Chauki H, Trouffleau D, Weiss M, Baret F, Brisson N (2003) Assimilating optical and radar data into the STICS crop model for wheat. *Agronomie* 23(4):297–303. <https://doi.org/10.1051/agro:2003003>
- Raun WR, Solie JB, Johnson GV, Stone ML, Lukina EV, Thomason WE, Schepers JS (2001) In-season prediction of potential grain yield in winter wheat using canopy reflectance. *Agron J* 93(1):131–138. <https://doi.org/10.2134/agronj2001.931131x>
- Ray DK, Gerber JS, MacDonald GK, West PC (2015) Climate variation explains a third of global crop yield variability. *Nat Commun* 6(1):5989. <https://doi.org/10.1038/ncomms6989>
- Sadeh Y, Cohen H, Maman S, Blumberg D (2018) Evaluation of manning's n roughness coefficient in arid environments by using SAR backscatter. *Remote Sens* 10(10):1505. <https://doi.org/10.3390/rs10101505>
- Sadeh Y, Zhu X, Chenu K, Dunkerley D (2019) Sowing date detection at the field scale using CubeSats remote sensing. *Comput Electron Agric* 157:568–580. <https://doi.org/10.1016/j.compag.2019.01.042>

- Sadeh Y, Zhu X, Dunkerley D, Walker JP, Zhang YX, Rozenstein O, Manivasagam VS, Chenu K (2021) Fusion of Sentinel-2 and PlanetScope time-series data into daily 3 m surface reflectance and wheat LAI monitoring. *Int J Appl Earth Obs Geoinf* 96:102260. <https://doi.org/10.1016/j.jag.2020.102260>
- Sagan V, Maimaitijiang M, Bhadra S, Maimaitiyiming M, Brown DR, Sidike P, Fritschi FB (2021) Field-scale crop yield prediction using multi-temporal WorldView-3 and PlanetScope satellite data and deep learning. *ISPRS J Photogramm Remote Sens* 174:265–281. <https://doi.org/10.1016/j.isprsjprs.2021.02.008>
- Sakamoto T, Yokozawa M, Toritani H, Shibayama M, Ishitsuka N, Ohno H (2005) A crop phenology detection method using time-series MODIS data. *Remote Sens Environ* 96(3–4):366–374. <https://doi.org/10.1016/j.rse.2005.03.008>
- Shang JL, Liu JG, Poncos V, Geng XY, Qian BD, Chen QH, Dong TF, Macdonald D, Martin T, Kovacs J, Walters D (2020) Detection of crop seeding and harvest through analysis of time-series Sentinel-1 interferometric SAR Data. *Remote Sens* 12(10):1551. <https://doi.org/10.3390/rs12101551>
- Shen JX, Evans FH (2021) The potential of Landsat NDVI sequences to explain wheat yield variation in fields in Western Australia. *Remote Sens* 13(11):2202. <https://doi.org/10.3390/rs13112202>
- Tian F, Wu J, Liu L, Leng S, Yang J, Zhao W, Shen Q (2019) Exceptional drought across Southeastern Australia caused by extreme lack of precipitation and its impacts on NDVI and SIF in 2018. *Remote Sens* 12(1):54. <https://doi.org/10.3390/rs12010054>
- Waldner F, Horan H, Chen Y, Hochman Z (2019) High temporal resolution of leaf area data improves empirical estimation of grain yield. *Sci Rep* 9(1):15714. <https://doi.org/10.1038/s41598-019-51715-7>
- Walker JP, Houser PR, Willgoose GR (2004) Active microwave remote sensing for soil moisture measurement: a field evaluation using ERS-2. *Hydrol Process* 18(11):1975–1997. <https://doi.org/10.1002/hyp.1343>
- Weiss M, Baret F (2016) S2ToolBox Level 2 products: LAI, FAPAR, FCOVER, version 1.1. In: ESA Contract n° 4000110612/14/I-BG (p. 52). INRA Avignon, France
- Zhang YX, Walker JP, Pauwels VRN, Sadeh Y (2022) Assimilation of wheat and soil states into the APSIM-wheat crop model: a case study. *Remote Sens* 14(1):65. <https://doi.org/10.3390/rs14010065>
- Zhao Y, Potgieter AB, Zhang M, Wu BF, Hammer GL (2020) Predicting wheat yield at the field scale by combining high-resolution Sentinel-2 satellite imagery and crop modelling. *Remote Sensing* 12(6):1024. <https://doi.org/10.3390/rs12061024>
- Zheng B, Chenu K, Fernanda Dreccer M, Chapman SC (2012) Breeding for the future: what are the potential impacts of future frost and heat events on sowing and flowering time requirements for Australian bread wheat (*Triticum aestivum*) varieties? *Glob Chang Biol* 18(9):2899–2914. <https://doi.org/10.1111/j.1365-2486.2012.02724.x>
- Zheng B, Chapman SC, Christopher JT, Frederiks TM, Chenu K (2015) Frost trends and their estimated impact on yield in the Australian wheatbelt. *J Exp Bot* 66(12):3611–3623. <https://doi.org/10.1093/jxb/erv163>
- Zheng BY, Chapman S, Chenu K (2018) The value of tactical adaptation to El Niño-Southern Oscillation for East Australian wheat. *Climate* 6(3):77. <https://doi.org/10.3390/cli6030077>

Publisher's Note Springer Nature remains neutral with regard to jurisdictional claims in published maps and institutional affiliations.